

Multi-scale wavelet coherence with its applications

Haibo Wu

Statistics Program, King Abdullah University of Science and Technology, K.S.A.

and

Marina I. Knight

Department of Mathematics, University of York, UK

and

Hernando Ombao

Statistics Program, King Abdullah University of Science and Technology, K.S.A.

May 19, 2023

Abstract

The goal in this paper is to develop a novel statistical approach to characterize functional interactions between channels in a brain network. Wavelets are effective for capturing transient properties of non-stationary signals because they have compact support that can be compressed or stretched according to the dynamic properties of the signal. Wavelets give a multi-scale decomposition of signals and thus can be few for studying potential cross-scale interactions between signals. To achieve this, we develop the scale-specific sub-processes of a multivariate locally stationary wavelet stochastic process. Under this proposed framework, a novel cross-scale dependence measure is developed. This provides a measure for dependence structure of components at different scales of multivariate time series. Extensive simulation studies are conducted to demonstrate that the theoretical properties hold in practice. The proposed cross-scale analysis is applied to the electroencephalogram (EEG) data to study alterations in the functional connectivity structure in children diagnosed with attention deficit hyperactivity disorder (ADHD). Our approach identified novel interesting cross-scale interactions between channels in the brain network. The proposed framework can be applied to other signals, which can also capture the statistical association between the stocks at different time scales.

Keywords: Non-stationary time series, Local stationarity, Scale-specific processes, Multi-resolution analysis, Wavelets process

1 Introduction

Electroencephalograms (EEGs) are recordings from the scalp that capture cortical brain electrical activity. Figure 1 shows the EEG data in a study involving healthy controls and those diagnosed with attention hyperactivity disorder (ADHD) (data reported in Motie Nasrabadi et al. (2020)). Due to their good temporal resolution (from hundreds of samples per second to thousands of samples per second), EEGs are useful for studying how different brain regions in the network interact with each other. In fact, functional brain connectivity serves as a potential biomarker for various neurological diseases (e.g., epilepsy, Alzheimer) and mental diseases (e.g., depression, obsessive-compulsive disorder and ADHD). However, analyzing brain signals is challenging because of their inherent non-stationarity. Hence, their statistical properties such as spectrum (or covariance), coherence (or correlation) evolve over time. The traditional Fourier methods are not sufficient in capturing transient properties of these signals. In this paper we develop a new framework, based on a discrete non-decimated wavelet transform, to overcome these limitations. Inspired by Nason et al. (2000) and Park et al. (2014), my proposed approach uses wavelets as building blocks for representing non-stationary time series. First, we use the multi-resolution property of wavelets to separate short-term from long-term dynamics in brain signals. Thus, one novel contribution of this paper is the introduction of the concept of scale-specific sub-processes derived from a more general formulation of a multivariate locally stationary wavelet process. The second goal is to examine multi-scale dependence across different sub-processes in order to identify how fluctuations in longer-term dynamics may have an impact on the amplitude of the shorter-term dynamics (or vice versa). Thus, the second novel contribution in this paper is the introduction of a new concept of cross-scale dependence in multivariate time series.

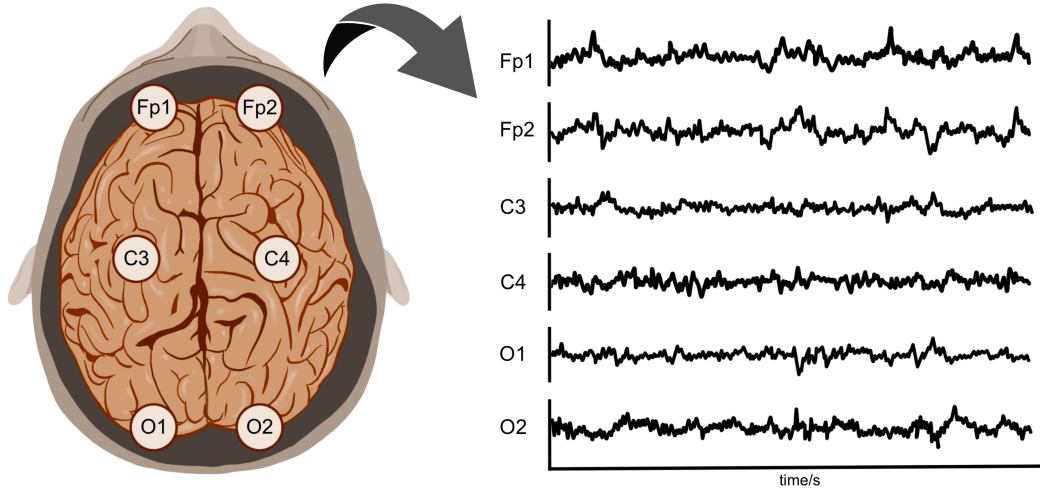


Figure 1: 10 seconds EEG signals recorded from 6 channels of a particular participant diagnosed with ADHD.

There has been a long history of statistical models for non-stationary time series. To generalize the Cramèr representation, Priestley (1981) and Dahlhaus (1997) proposed a linear mixture of Fourier waveforms with random amplitudes that vary across time. In Ombao et al. (2005), a model that uses the library of smooth localized complex exponentials (SLEX) is proposed. As an alternative to the Fourier representation of signals, Nason et al. (2000) introduced a stochastic process that uses discrete wavelets as its building blocks. Under the proposed locally stationary wavelet model, the evolutionary wavelet spectrum was introduced. A special framework in Sanderson et al. (2010) was developed to estimate the wavelet coherence of bivariate nonstationary time series. In Park et al. (2014), the multivariate locally stationary wavelet process (MvLSW) was developed and the notions of coherence and partial coherence across multiple channels were introduced. The framework in Fiecas and Ombao (2016) extends the Dahlhaus model to the case where there are several trials but assume that the signals are uncorrelated across trias. The locally stationary

wavelets alternative was developed in Embleton et al. (2022) and additionally allowed for dependence across the time line of the ordered trials. These Fourier and wavelet stochastic representations all share a common feature: the random coefficients are uncorrelated across frequencies (in the Fourier case) or across scales and time-shifts (in the wavelets case, see Figure 2(a)). This is a serious limitation especially when one aims to study the dependence between short-term and long-term process dynamics.

In this paper we propose a novel modelling framework to capture the cross-scale dependence structure between the multivariate non-stationary time series. As noted, the current MvLSW model developed by Park et al. (2014) assumes that the random innovations across different scales are uncorrelated. In contrast, our proposed construction differs from existing work through the introduction of a new, relaxed assumption for the process random coefficients that in effect allows for cross-scale (or multi-scale) dependence (Figure 2(b)) gives a visual representation for cross-scale dependence).

The proposed framework also provides the theory for (a.) defining the cross-scale local wavelet spectrum, cross-scale local cross-covariance and cross-correlation; and (b.) rigorous inference on these unknown quantities. The primary contribution of our proposed framework is that it can help us to measure and estimate the cross-scale dependence, which can not be realized by other previous approaches. Specifically, by measuring the cross-scale dependence structures between brain signals from different channels, new inference about interactions among different brain regions can be carried out. One potential impact of this new tool is that it will enable neuroscientists to examine how long-term brain dynamics in one channel can impact short-term brain dynamics in another channel. This will be potentially useful to study associations between brain connectivity and cognitive functions; and the potential roles of altered brain connectivity in the development and progression

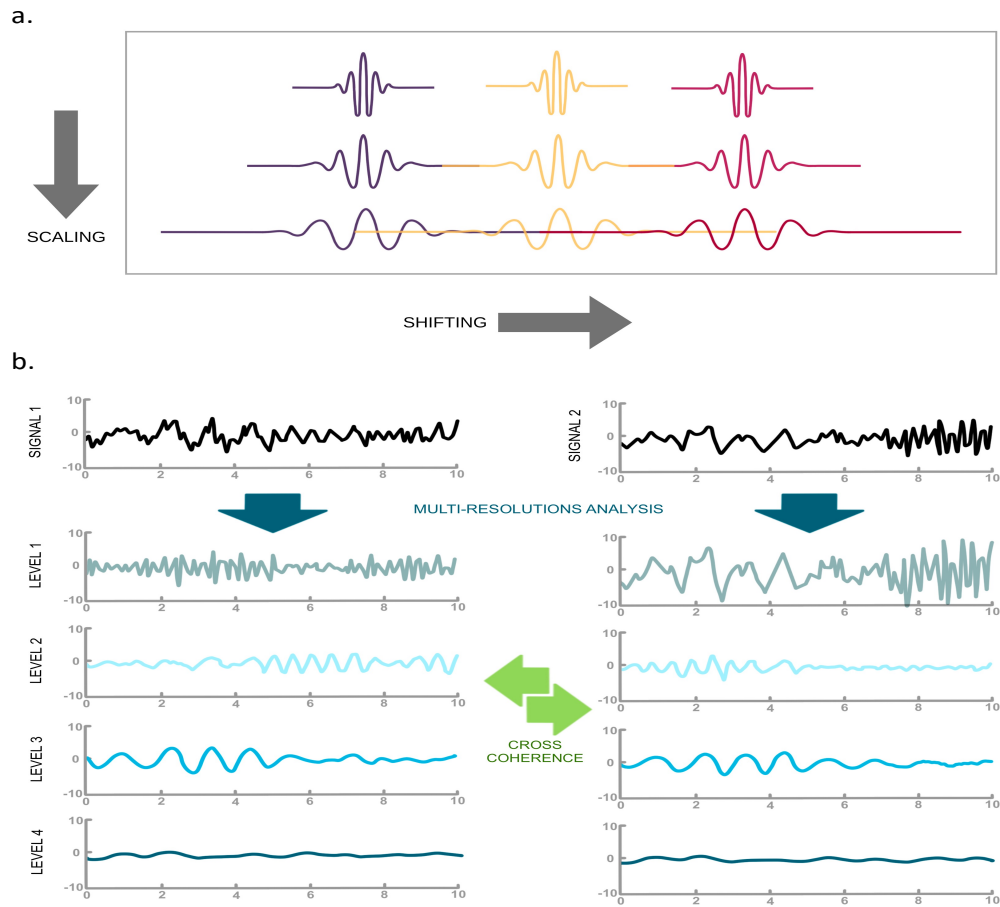


Figure 2: (a) shows the Morlet wavelet at different scales and locations; (b) shows Two non-stationary time series and their components at scale= 1, ..., 4.

of neurological and mental diseases. In addition to neuroscience, the proposed tool can be applied to other types of time series data. The systemic risk of the financial system got much attention in recent research like Basu et al. (2019), the framework also provides a new approach to identify the interconnectedness structure of the stocks, allowing us to determine the specific time scale that contains the crucial information.

The format of the paper is as follows. Section 2.1 and Section 2.2 give a brief introduction on wavelets and the multivariate locally stationary wavelet process previously proposed by Park et al. (2014). Section 2.3 develops our scale-specific multivariate locally stationary wavelet process with cross-scale dependence structure. A measure of cross-scale dependence is introduced in the Section 2.4. Section 3 gives simulation studies to illustrate the practical effects and advantages of the proposed modelling approach. Section 4.1 details the application of the proposed methodologies to a real EEG data, and we crucially compare the dependence structures between the patient group and control group. Section 4.2 is the application of the framework to the financial data. Section 5 concludes the paper.

2 Novel scale-specific nonstationary subprocesses

The framework proposed in this section is for measuring cross-dependence among multivariate nonstationary time series at different resolution scales, and capturing the frequency information of the subprocesses at the scales that cause high dependence. Multiresolution analysis (MRA, see e.g., Daubechies (1992)) provides the theoretical foundation for deriving such subprocesses at every scale. These ideas suggest that a time series X_t can be represented a sum of ‘smooth’ and ‘detailed’ components. This construction will be examined in greater detail in the following subsections.

2.1 Brief introduction of wavelets

We first give a brief introduction of wavelets by contrasting them to Fourier constructions. Fourier analysis is a fundamental tool in studying stationary time series because it identifies the frequencies of random oscillations that dominate the signal. However, classical Fourier analysis assumes that the time series is stationary. Intuitively, this means that the oscillatory content of the signal and spectrum remains constant over time. Thus, Fourier constructions cannot be directly used to study signals whose oscillatory content changes with time. For non-stationary signals, it is ideal to instead consider wavelets which are known to have good time-localization properties. Wavelets are generated from some special functions, one typically referred to as the father wavelet, ϕ , which integrates to one and is used to capture the smooth, low frequency nature of the time series; another one is called the mother wavelet, ψ , which integrates to zero and is used to capture the detailed, high frequency information of the data. The mother wavelets are compressed and then shifted to produce ‘children’ wavelets (see Figure 2.a). The wavelets functions at scale j and shift k , denoted by $\psi_{j,k}$, are generated from the mother wavelet, ψ , and are defined as

$$\psi_{j,k}(t) = 2^{-j/2} \psi\left(\frac{t - 2^j k}{2^j}\right), \quad j = 1, \dots, J$$

where J is the number of scales. Similar constructions for the father wavelet, denoted by $\phi_{j,k}$, are typically known as scaling functions. The scales $j = 1, \dots, J$ indicate the signal resolution and further wavelet properties, such as orthonormality appear in e.g., Daubechies (1992).

2.2 Summary of locally stationary wavelet processes

First, a brief description of key features of the *locally stationary wavelet* (LSW) framework is presented. Suppose that $\{X(t)\}$ is a univariate non-stationary time series. A basic

formulation for the orthogonal wavelet decomposition of a time series in the notation above is

$$X(t) = \sum_{k \in \mathbb{Z}} s_{J,k} \phi_{J,k}(t) + \sum_{k \in \mathbb{Z}} d_{J,k} \psi_{J,k}(t) + \sum_{k \in \mathbb{Z}} d_{J-1,k} \psi_{J-1,k}(t) + \dots + \sum_{k \in \mathbb{Z}} d_{1,k} \psi_{1,k}(t)$$

where $s_{J,k}$ and $d_{j,k}$ are the coefficients of father wavelet and mother wavelet respectively at the corresponding scales and shifts. The LSW model proposed by Nason et al. (2000) gives a discrete non-decimated wavelets representation of a discretely sampled non-stationary time series with time-varying second order structures, where the non-decimated wavelet is shift-invariant because it eliminates the downsampling and consequently, is more appropriate for identifying both stationary and non-stationary behaviors in signals (Brassarote et al. (2018)). Under this framework, it provides a time-localized wavelet spectrum which is estimated using a wavelet periodogram. Specifically, for $T = 2^J$ for $J \in \mathbb{N}$, a sequence of (doubly-indexed) stochastic processes, $\{X_{t;T}\}$, is defined to be a LSW process if it has following representation in the mean-square sense:

$$X_{t;T} = \sum_{j=1}^{\infty} \sum_{k \in \mathbb{Z}} W_j(k/T) \psi_{j,k}(t) \xi_{j,k} \quad (1)$$

where for scale j and shift k , $W_j(k/T)$ is a smoothly varying transfer function corresponding to the discrete non-decimated wavelet $\psi_{j,k}$ and $\{\xi_{j,k}\}$ are a collection of zero-mean, unit-variance uncorrelated random variables. Here, $\{W_j(\cdot)\}$ are assumed to be a smoothly varying continuous Lipschitz function for ensuring that transfer functions can be estimated locally. The transfer function $W_j(k/T)$ measures the time-varying contribution to the variance of the overall process. Consequently, the evolutionary wavelet spectrum (EWS) is defined as $S_j(z) = |W_j(z)|^2$, to describe the power at given scale j and rescaled time points z , where $z = k/T \in (0, 1)$. The multivariate LSW (MvLSW) process of Park et al. (2014) is based on the above original single-replicate formulation, which allows

us to estimate the dependence – at the same scale – between time series data recorded from different channels. The P -dimensional locally stationary wavelet process $\{\mathbf{X}_{t;T}\}$ with $\mathbf{X}_{t;T} = [X_{t;T}^{(1)}, X_{t;T}^{(2)}, \dots, X_{t;T}^{(P)}]'$, has the form

$$\mathbf{X}_{t;T} = \sum_{j=1}^{\infty} \sum_k \mathbf{V}_j(k/T) \psi_{j,t-k} \mathbf{z}_{j,k} \quad (2)$$

where $\mathbf{V}_j(k/T)$ is a $P \times P$ transfer function matrix assumed to have a lower-triangular form; $\{\psi_{j,t-k}\}_{jk}$ is a set of discrete non-decimated wavelets; $\{\mathbf{z}_{j,k}\}$ is a set of uncorrelated random vectors with mean vector $\mathbf{0}$ and $P \times P$ identity covariance matrix. The covariance of these random innovations in the basic LSW model is defined as $cov(z_{j,k}^{(i)}, z_{j',k'}^{(i')}) = \delta_{i,i'} \delta_{j,j'} \delta_{k,k'}$, which means that the uncorrelation holds not only across different times $k \neq k'$, but also at different scales $j \neq j'$ and channels $i \neq i'$. In particular, if $j = j'$, $i = i'$ and $k = k'$, then the covariance of these random innovations is a identity matrix. In Sanderson et al. (2010) and Embleton et al. (2022), the wavelet spectral matrix is estimated by wavelet periodogram. In this thesis, we abandon these strict assumptions and introduce a dependence function between the innovations that will enable us to capture the dependence between channels at different scales. This is discussed further in Section 2.3 next.

2.3 Novel Multivariate LSW and Subprocesses

A significant limitation of the previous models is the assumption that the process random innovations at different scales are uncorrelated. The major novelty of our framework is that it provides a measure for potential cross-scale (multi-scale) dependence structure between multivariate time series, although the cross-scale dependence could be naturally weak at many cases.

DEFINITION 1 Considering a P -variate stochastic time series, $\{\mathbf{X}_{t;T}\}_{t=0,1,\dots,T}$, where $T = 2^{J(T)}$ to be a multivariate locally stationary wavelet process with cross-scale dependence if

it has the representation,

$$\mathbf{X}_{t;T} = \sum_{j=1}^{\infty} \sum_{k \in \mathbb{Z}} \mathbf{V}_j(k/T) \psi_{j,k}(t) \mathbf{z}_{j,k} \quad (3)$$

where $\{\psi_{j,k}\}$ is a set of discrete non-decimated wavelets; $\mathbf{V}_j(k/T)$ is the $P \times P$ transfer function matrix, with an assumption that each element of the matrix is a Lipschitz continuous function whose corresponding Lipschitz constant, $L_j^{(p,q)}$ for channels (p, q) , collectively admit $\sum_{j=1}^{\infty} 2^j L_j^{(p,q)} < \infty$; $\{\mathbf{z}_{j,k}\} = \{[z_{j,k}^{(1)}, \dots, z_{j,k}^{(P)}]\}$ is a collection of $P \times 1$ random vectors. We assume that: (a) for all j, k , $E[\mathbf{z}_{j,k}] = 0$; (b) the covariance $cov(\mathbf{z}_{j,k}, \mathbf{z}_{j',k'}) = \delta_{k,k'} \mathbf{Q}_{j,j';k}$, where $\{\mathbf{Q}_{j,j';k}\}_k$ determine the correlation between random vectors at scales j and j' , at each time location k , which is a $P \times P$ matrix; (c) $\mathbf{Q} = \mathbf{I}$ if and only if $j = j'$, which is an identity matrix; (d) For the (p, q) element of \mathbf{Q} with time shift k , $Q_{j,j';k}^{(p,q)}$, which can be obtained by $Q_{j,j';k}^{(p,q)} = cov(z_{j,k}^{(p)}, z_{j',k}^{(q)})$.

REMARK: The cross-scale dependence function fulfills $|Q_{j,j';k}^{(p,q)}| \leq 1$ for all $j, j', k, (p, q)$. The assumption of uncorrelated scales amounts to $Q_{j,j';k}^{(p,q)} = \delta_{j,j'}$.

DEFINITION 2 From (3) we define the sub-process of MvLSW process with cross-scale dependence as the scale- j component P -variate locally stationary wavelet process, $\mathbf{X}_{j,t} = [X_{j,t}^{(1)}, \dots, X_{j,t}^{(P)}]'$, with the following representation,

$$\mathbf{X}_{j,t} = \sum_{k \in \mathbb{Z}} \mathbf{V}_j(k/T) \psi_{j,k}(t) \mathbf{z}_{j,k} \quad (4)$$

where $\mathbf{V}_j(k/T)$, $\psi_{j,k}$ and $\mathbf{z}_{j,k}$ follow the definition and assumptions of Definition 1. $X_j^{(p)}$ represents the scale- j representation of the original channel p process, $X_{t;T}^{(p)}$. By multi-resolution properties, we have the approximation $X_{t;T}^{(p)} = \sum_j X_{j,t}^{(p)}$. The cross-scale dependence we measure is the coherence between the subprocesses, $\rho_{jj'}^{(p,q)}$, where

$$\rho_{jj'}^{(p,q)} = |corr(X_{j,t}^{(p)}, X_{j',t+\tau}^{(q)})|^2 \quad (5)$$

DEFINITION 3 Let $\{\mathbf{X}_{t,T}\}$ be a MvLSW time series with cross-scale dependence structure as in Definition 1. Suppose that $\mathbf{V}_j(u)$ and $\mathbf{V}_{j'}(u)$ are scale-specific (j and j') time-dependent ($u = t/T, t = 0, 1, \dots, T-1$) transfer function matrices corresponding to scale- j and scale- j' components of $\mathbf{X}_{t,T}$ respectively, then the *cross-scale local wavelet spectral matrix* (cross-scale LWS) for any pair of scales (j, j') and rescaled time point u is defined as,

$$\mathbf{S}_{jj'}(u) = \mathbf{V}_j(u)\mathbf{Q}_{jj'}(u)\mathbf{V}'_{j'}(u) \quad (6)$$

where \prime denotes matrix transposition. If $j = j'$, then $\mathbf{S}_{jj'}(u) = \mathbf{S}_j(u)$ and coincides with the definition of Park et al. (2014).

REMARK: The cross-scale LWS matrix provides a measure of local contribution to cross-scale covariance between channels at a given time point u , and a pair of scale (j, j') . Compared with the single scale LWS matrix, $\mathbf{S}_j(u)$, the cross-scale LWS matrix does not have a symmetric structure if $j \neq j'$. The diagonal elements of the cross-scale LWS matrix are the individual channel spectra and are denoted $S_{jj'}^{(p,p)}(u)$. The off-diagonal terms, $S_{jj'}^{(p,q)}(u)$, describe the cross-spectrum between channels p and q at a given pair of scales (j, j') .

2.4 Cross-scale covariance and coherence

In this section we develop novel quantities that allow us to measure the dependence structure between the MvLSW sub-processes at different scales, and discuss the connection between the cross-scale LWS matrix and the local auto- and cross-scale covariance.

DEFINITION 4 For any pair of scales $j, j' \in \mathbb{N}$, time k and lag $\tau \in \mathbb{Z}$, the cross-scale autocorrelation wavelets (Embleton et al., 2022) can be defined as,

$$\Psi_{jj'}(\tau) = \sum_{k \in \mathbb{Z}} \psi_{j,k}(0)\psi_{j',k}(\tau). \quad (7)$$

DEFINITION 5.1 Define the operator $A_{jj';ll'}$ by

$$A_{jj';ll'} := \langle \Psi_{jj'}, \Psi_{ll'} \rangle = \sum_{\tau \in \mathbb{Z}} \Psi_{jj'}(\tau) \Psi_{ll'}(\tau). \quad (8)$$

DEFINITION 5.2 Define the operator $A_{jj';ll'}^\delta$ by

$$A_{jj';ll'}^\delta := \sum_{\tau \in \mathbb{Z}} \Psi_{jj'}(\tau) \Psi_{ll'}(\tau + \delta). \quad (9)$$

REMARK: If $j = j'$, then $\Psi_{jj}(\tau) = \Psi_j(\tau)$, where $\Psi_j(\tau)$ is the autocorrelation wavelet defined by Nason et al. (2000). It can be shown that $A_{jj';ll'} = A_{jl;j'l'}$. Clearly, $A_{jj';ll'} = A_{jj';ll'}^0$. The operator $A_{jj';ll'}^\delta$ is invertible and for each pair of scales the norm of $A_{jj';ll'}^\delta$ is bounded from above by some constant C .

DEFINITION 6 For a given scale j and rescaled time u , let $c_j^{(p,p)}(u, \tau)$ denote the scale-specific local autocovariance of channel p at lag τ and $c_j^{(p,q)}(u, \tau)$ be the scale-specific local cross-covariance between channels p and q . In terms of the local auto- and cross-covariance functions defined by Park et al. (2014), we define these in terms of the elements of the cross-scale LWS matrix and of the cross-scale autocorrelation wavelets, as following representations,

$$\begin{aligned} c_j^{(p,p)}(u, \tau) &= S_j^{(p,p)}(u) \Psi_j(\tau), \\ c_j^{(p,q)}(u, \tau) &= S_j^{(p,q)}(u) \Psi_j(\tau). \end{aligned} \quad (10)$$

DEFINITION 7 For a given pair of scales (j, j') and rescaled time u , let $c_{jj'}^{(p,p)}(u, \tau)$ denote the dual-scale local autocovariance of channel p at lag τ and $c_{jj'}^{(p,q)}(u, \tau)$ be the dual-scale local cross-covariance between channels p and q . We define these functions in terms of the elements of cross-scale LWS matrix and the cross-scale autocorrelation wavelets, as following representations,

$$\begin{aligned} c_{jj'}^{(p,p)}(u, \tau) &= S_{jj'}^{(p,p)}(u) \Psi_{jj'}(\tau), \\ c_{jj'}^{(p,q)}(u, \tau) &= S_{jj'}^{(p,q)}(u) \Psi_{jj'}(\tau). \end{aligned} \quad (11)$$

REMARK: If the scales coincide ($j = j'$), then $c_{jj'}^{(p,p)}(u, \tau) = c_j^{(p,p)}(u, \tau)$ and $c_{jj'}^{(p,q)}(u, \tau) = c_j^{(p,q)}(u, \tau)$. Then we consider if under this definition the dual-scale local auto- and cross-covariance functions exactly represent the covariance between scale-specific sub-processes of the signals.

PROPOSITION 1: Let $c_j^{(p,q)}(u, \tau)$ denote the scale-specific local cross-covariance from Definition 4 and $c_{jj'}^{(p,q)}(u, \tau)$ denote the dual-scale local cross-covariance from Definition 5. Then, asymptotically, these functions can be approximately represented in terms of the covariance between the scale-specific sub-processes, namely,

$$\begin{aligned} \left| \text{cov}(X_{j,[uT]}^{(p)}, X_{j,[uT]+\tau}^{(q)}) - c_j^{(p,q)}(u, \tau) \right| &= \mathcal{O}(T^{-1}) \\ \left| \text{cov}(X_{j,[uT]}^{(p)}, X_{j',[uT]+\tau}^{(q)}) - c_{jj'}^{(p,q)}(u, \tau) \right| &= \mathcal{O}(T^{-1}). \end{aligned}$$

PROOF: See Appendix.

We now provide a measure of cross-scale dependence between different channels at a given pair of scales. This dependence can be quantified by defining the cross-scale wavelet coherence between channels.

DEFINITION 8 For any pair of scales (j, j') and rescaled time $u \in (0, 1)$, the dual-scale wavelet coherence matrix, $\boldsymbol{\rho}_{jj'}(u)$ is defined as,

$$\boldsymbol{\rho}_{jj'}(u) = \mathbf{D}_j(u) \mathbf{S}_{jj'}(u) \mathbf{D}_{j'}(u) \quad (12)$$

The matrices $\mathbf{D}_j(u)$, $\mathbf{D}_{j'}(u)$ are diagonal with elements $S_{jj}^{(p,p)}(u)^{(-1/2)}$ and $S_{j'j'}^{(q,q)}(u)^{(-1/2)}$ respectively, as previously defined by Park et al. (2014). The (p, q) element of the wavelet coherence matrix, $\rho_{jj'}^{(p,q)}(u)$, is the dual-scale coherence between scale j - channel p and scale j' - channel q , which can be expressed as,

$$\rho_{jj'}^{(p,q)}(u) = \frac{S_{jj'}^{(p,q)}(u)}{\sqrt{S_{jj}^{(p,p)}(u) S_{j'j'}^{(q,q)}(u)}} \quad (13)$$

REMARK: $\rho_{jj'}^{(p,q)}(u)$ is a cross-scale dependence function taking a value between -1 and 1 at any given time u , determined by the cross-scale dependence structure of the multivariate process. A value close to ± 1 indicates a strong cross-scale linear dependence between channels at given time and scale.

2.5 Estimation theory

In this section we pay attention to the estimation of the spectral quantities associated to the proposed MvLSW with cross-scale dependence framework. We start from considering the estimation of the cross-scale LWS matrix which was defined in Section 2.3.

First, we introduce the *empirical wavelet coefficient vector*, $\mathbf{d}_{j,k} = [d_{j,k}^{(1)}, \dots, d_{j,k}^{(P)}]'$, defined by Park et al. (2014) as $\mathbf{d}_{j,k;T} = \frac{1}{\sqrt{T}} \sum_{t=0}^{T-1} \mathbf{X}_{t;T} \psi_{jk}(t)$, then we define the *cross-scale wavelet periodogram matrix*, $\mathbf{I}_{jj',kk'}$ as,

$$\mathbf{I}_{jj',kk'} = \mathbf{d}_{j,k} \mathbf{d}'_{j',k'},$$

where for ease of notation we dropped the T subscript.

In the above, we denote by $I_{jj',kk'}^{(p,q)}$ the (p, q) entry of the cross-scale periodogram matrix at a given pair of scales (j, j') , where $p, q \in \{1, \dots, P\}$. We start from this raw cross-scale wavelet periodogram matrix to explore a final estimator with the desired asymptotic properties.

PROPOSITION 2: Let $\{\mathbf{X}_{t;T}\}$ be a MvLSW time series with cross-scale dependence structure and underlying cross-scale LWS matrix denoted $\mathbf{S}_{jj'}(u)$ at rescaled time u . Then,

asymptotically for any times k, k' and cross-scale (j, j') ,

$$\begin{aligned}
E[\mathbf{I}_{jj',kk'}] &= \sum_l \sum_{l'} A_{ll';jj'}^{k-k'} \mathbf{S}_{ll'}(k/T) + \mathcal{O}(T^{-1}) \quad \text{and} \\
\text{var}(I_{jj',kk'}^{(p,q)}) &= \sum_l \sum_{l'} A_{ll';jj'}^{k-k'} S_{ll'}^{(p,p)}(k/T) \sum_l \sum_{l'} A_{ll';jj'}^{k-k'} S_{ll'}^{(q,q)}(k/T) \\
&\quad + \left(\sum_l \sum_{l'} A_{ll';jj'}^{k-k'} S_{ll'}^{(p,q)}(k/T) \right)^2 + \mathcal{O}(2^{2j}/T), \quad \forall (p, q)
\end{aligned}$$

PROOF: See Appendix.

The above results indicate that the raw wavelet periodogram matrix is both asymptotically biased and inconsistent. The inner product matrix \mathbf{A} is established to be invertible for all Daubechies' wavelets and is the main reason behind the bias. The usual approach to solve this problem, which we also adopt here, is to smooth the raw cross-scale wavelet periodogram and then correct the bias (Nason et al., 2000). In a similar vein to Embleton et al. (2022), we apply a rectangular kernel smoother with window of length $(2M + 1)$ across time to smooth the raw periodogram, yielding

$$\tilde{\mathbf{I}}_{jj',kk'} = \frac{1}{2M + 1} \sum_{m=-M}^M \mathbf{I}_{jj',(k+m)(k'+m)}. \quad (14)$$

PROPOSITION 3: The above estimator has the following asymptotic properties,

$$\begin{aligned}
E[\tilde{I}_{jj',kk'}^{(p,q)}] &= \sum_l \sum_{l'} A_{ll';jj'}^{k-k'} S_{ll'}(k/T) + \mathcal{O}(MT^{-1}) + \mathcal{O}(T^{-1}) \\
\text{var}(\tilde{I}_{jj',kk'}^{(p,q)}) &= \mathcal{O}(2^{2j}/M) + \mathcal{O}(2^{2j}/T) + \mathcal{O}(2^{2j'}/M) + \mathcal{O}(2^{2j'}/T)
\end{aligned}$$

PROOF: See Appendix.

REMARK: In the limit, as $T, M \rightarrow \infty$, $\text{var}(\tilde{I}_{jj',kk'}^{(p,q)}) \rightarrow 0$. There is a trade-off observed between bias and variance: increasing M reduces the variance but also increases the bias.

An additional condition that $M/T \rightarrow 0$ is necessary, ensuring $\left| E[\tilde{I}_{jj',kk'}^{(p,q)}] - E[I_{jj',kk'}^{(p,q)}] \right| \rightarrow 0$.

We next correct the smoothed cross-scale periodogram matrix for bias using the inverse of

the inner product matrix \mathbf{A}^{-1} . The final smoothed unbiased estimator of the cross-scale LWS matrix is given by

$$\hat{\mathbf{S}}_{jj'}(u) = \sum_{l=1}^J \sum_{l'=1}^J \left(A_{ll';jj'}^{k-k'} \right)^{-1} \tilde{I}_{ll',kk'} \quad (15)$$

The quantity $\hat{\mathbf{S}}_{jj'}(k/T)$ can be used to estimate the cross-scale wavelet coherence. Denote the (p, q) -th entry of $\hat{\mathbf{S}}_{jj'}(k/T)$ to be $\hat{S}_{jj'}^{(p,q)}(k/T)$ and let $\hat{\mathbf{D}}_j(k/T)$, $\hat{\mathbf{D}}_{j'}(k/T)$ are diagonal matrix whose elements are $(\hat{S}_j^{(p,p)}(k/T))^{-(1/2)}$ and $(\hat{S}_{j'}^{(p,p)}(k/T))^{-(1/2)}$ respectively. Then we define the estimator of the cross-scale wavelet coherence matrix to be,

$$\hat{\boldsymbol{\rho}}_{jj'}(k/T) = \frac{\hat{\mathbf{S}}_{jj'}(k/T)}{\sqrt{\hat{\mathbf{S}}_{jj}(k/T)\hat{\mathbf{S}}_{j'j'}(k/T)}} \quad (16)$$

The (p, q) -th element of the $\hat{\boldsymbol{\rho}}_{jj'}(k/T)$ is the estimated time-varying cross-scale wavelet coherence between channels p and q at a given pair of scales (j, j') .

3 Simulation Study

To illustrate our proposed model that multivariate locally stationary wavelet process (MvLSW) with cross-scale dependence structure, we now consider the simulation study. We simulate time series using a tri-variate model with the following form, $\mathbf{X}_t = [X_t^{(1)}, X_t^{(2)}, X_t^{(3)}]'$. Specifically, by generating three 10 seconds 100Hz time series from latent processes, $Z_1(t)$, $Z_2(t)$, $Z_3(t)$, with the form as,

$$Z_1(t) = \phi_{11}Z_1(t-1) + \phi_{12}Z_1(t-2) + w_{1t},$$

$$Z_2(t) = \phi_{21}Z_2(t-1) + \phi_{22}Z_2(t-2) + w_{2t},$$

$$Z_3(t) = \phi_{31}Z_3(t-1) + \phi_{32}Z_3(t-2) + w_{3t}$$

where $\phi_{11} = \frac{2\cos(2\pi\eta_1)}{M_1}$, $\phi_{12} = -\frac{1}{M_1^2}$, $\phi_{21} = \frac{2\cos(2\pi\eta_2)}{M_2}$, $\phi_{22} = -\frac{1}{M_2^2}$, $\phi_{31} = \frac{2\cos(2\pi\eta_3)}{M_3}$, $\phi_{32} = -\frac{1}{M_3^2}$, and $M_1 = 1.05$, $M_2 = 1.01$, $M_3 = 1.05$, $\eta_1 = 0.375$, $\eta_2 = 0.19$, $\eta_3 = 0.09$, $\mathbf{w}_t =$

$[w_{1t}, w_{2t}, w_{3t}]'$ is time-varying so that the cross dependence structure changes over the time.

The parameters make the power of the processes concentrate on corresponding frequency

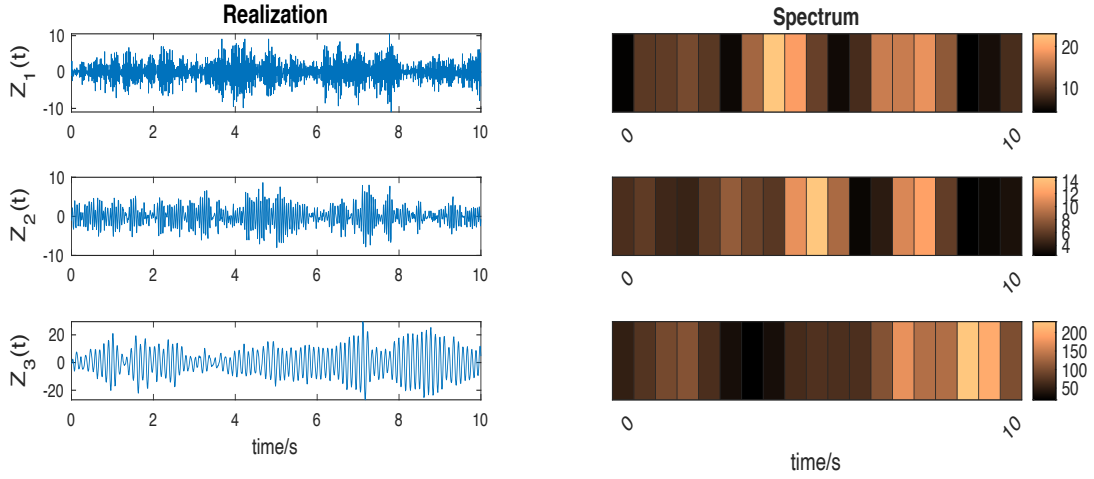


Figure 3: The realization and time-varying wavelet spectrum of $Z_1(t)$, $Z_2(t)$ and $Z_3(t)$.

bands (see Figure 3), the structure is such that: for $Z_1(t)$, there is a peak in the spectral power at $37.5Hz$ which corresponds to wavelet subprocess at level $j = 1$; for $Z_2(t)$, the peak of spectrum is at $19Hz$ which corresponds to the mid point of wavelet level $j = 2$; for $Z_3(t)$, the peak of spectrum is at $9Hz$ that corresponds to the wavelet process at level $j = 3$. \mathbf{X}_t is the linear combination of above three latent processes with time-varying coefficients, with following representations, $X_t^{(1)} = 0.5Z_1(t) + 0.5Z_3(t)$, $0 < t < 10$, and

$$X_t^{(2)} = \begin{cases} 0.9Z_1(t) + 0.1Z_2(t), & 0 < t < 5 \\ 0.1Z_1(t) + 0.9Z_2(t), & 5 < t < 10 \end{cases}$$

$$X_t^{(3)} = \begin{cases} 0.9Z_3(t) + 0.1Z_1(t), & 0 < t < 5 \\ 0.9Z_1(t) + 0.1Z_3(t), & 5 < t < 10 \end{cases}$$

100 tri-variate signals were simulated from this model, and using the framework proposed in Section 2 we calculate the cross-scale coherence of the subprocesses of the simulated signals given several different pair of scales. The spectrum of each signal is also compute

to determine if this framework can capture the components that cause the dependence between the time series.

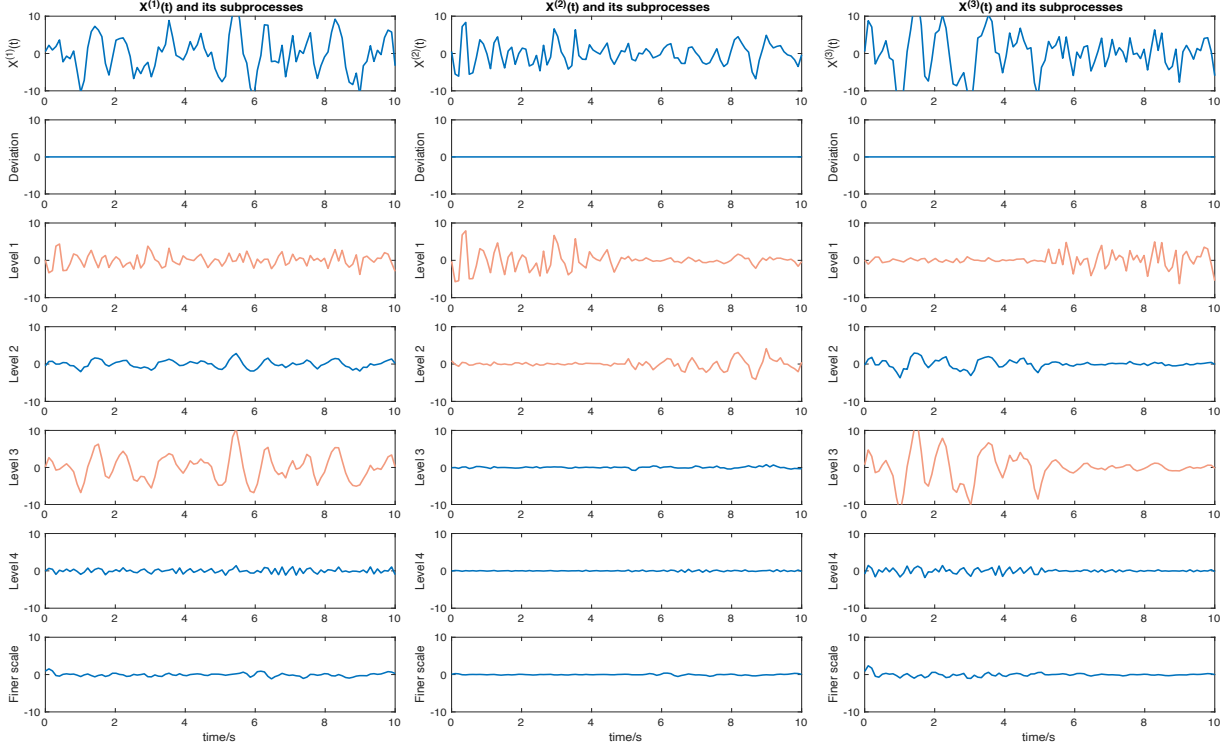


Figure 4: The realization of $X_t^{(1)}, X_t^{(2)}$ and $X_t^{(3)}$ and their subprocesses at every scale; Deviation denotes the difference between the original signal and sum of subprocesses at every scale.

Figure 4 shows the realizations of $X_t^{(1)}, X_t^{(2)}, X_t^{(3)}$ and their subprocesses at every scale, the Figure 5 shows the corresponding spectrum. Here $J = 4$ is the decomposition level, then we can get the subprocesses at scale $j = 1, \dots, 4$ and father wavelet. Through the results of power spectrum, the components the signals contained can be accurately captured by the subprocess at corresponding scale.

Figure 6(b) shows the results of the single-scale coherence, we calculate this by a 50 time points moving window with a 10 time points step. $X_j^{(p)}(t)$ denotes the scale- j component of \mathbf{X}_t from channel p . $X_1^{(1)}$ and $X_1^{(2)}$ have strong dependence during 0s to 5s, which

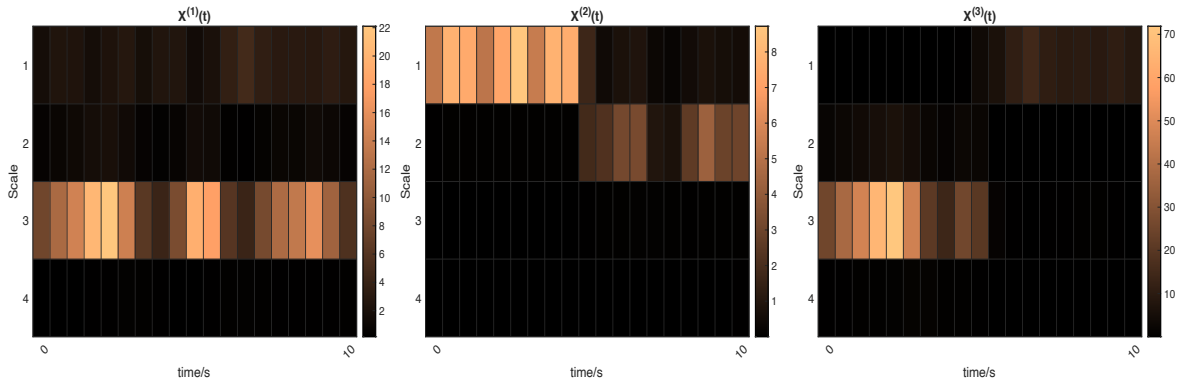


Figure 5: The time-varying wavelet spectrum of $X_t^{(1)}$, $X_t^{(2)}$ and $X_t^{(3)}$ at every scale.

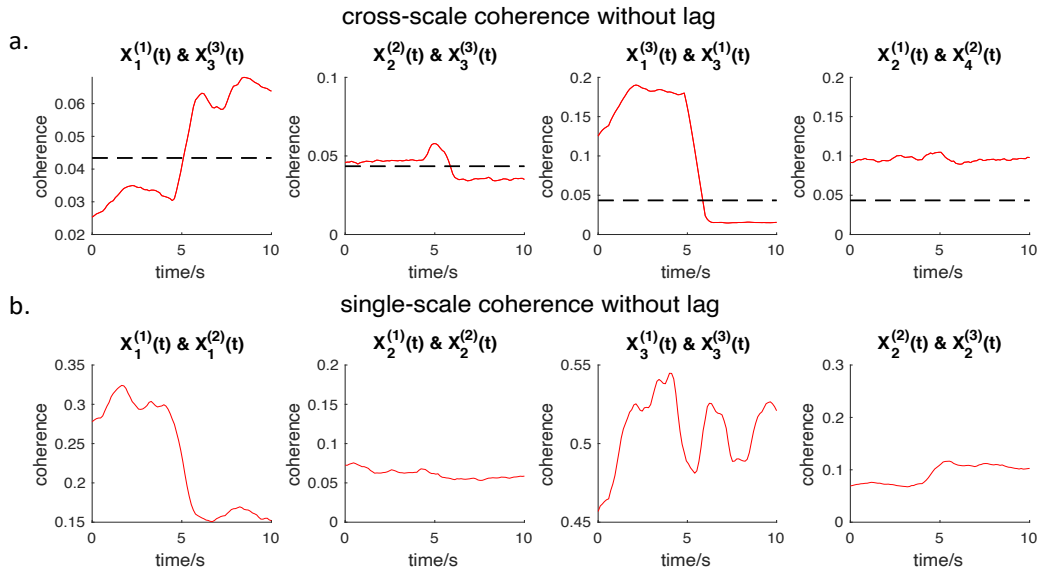


Figure 6: (a) shows mean of truth coherence (red solid) between some subprocesses at the different scales obtained from 100 simulations, and the dotted lines denote the threshold under 99% confidence level. (b) shows that of same scales.

corresponds to the results in the Figure 4 because the subprocesses contain the components at the same frequency band during 0s to 5s. The coherence between $X_2^{(1)}(t)$ and $X_2^{(2)}(t)$ is weak because of dissimilar components, the similar results found in coherence between $X_2^{(2)}(t)$ and $X_2^{(3)}(t)$. In the other hand, for the cross-scale coherence between $X_3^{(1)}(t)$ and $X_1^{(3)}$ has higher values over 0s to 5s because they contain same components during this period, and then sharply drop to zero at around 5s. In comparison, the coherence between $X_1^{(1)}$ and $X_3^{(3)}$ is weak from 0s to 5s, and considerably increasing to around 0.1. Additionally, some subprocesses do not exhibit cross-scale dependence, such as $X_2^{(2)}, X_3^{(3)}$ shown in Figure 6(a). For determining whether the coherence between the subprocesses at difference scale is statistical significant, a hypothesis test procedure performed with the generated time series: (1) the null hypothesis H_0 is that the the cross-scale coherence $\rho_{jj'} = 0$; (2) 100,000 time series are generated under H_0 to obtain the empirical distribution of $\hat{\rho}_{jj'}$, specifically, we have $\mathbf{X}(t) = \sum_{j=1}^J \sum_k \mathbf{V}_j(k/T) \psi_{j,t-k} \mathbf{z}_{j,k}$, where decomposition level, $J = 5$ and the length of time series, $T = 1000$; $V_j(k/T)$ is still time-varying transfer function matrix; $\psi_{j,k}$ is non-decimated wavelet with the same type as the simulation study; $\mathbf{z}_{j,k} \sim N(0, \mathbf{I})$ and $cov(z_{j,k}, z_{j',k}) = 0$. Figure 7 shows the results of hypothesis test under the H_0 , compared to cross-scale coherence obtained with simulation data, it illustrates that for the MvLSW process, the cross-scale dependence significantly exists among some pair of subprocesses at many time periods, although in most of case it weaker than the single scale dependence. The same components contained in the time series can be capture by our framework.

To investigate if our framework can identify how fluctuations in longer-term dynamics may have an impact on the amplitude of the shorter-term dynamics, we calculate the cross-scale with lag time (0.6s and 1s) on simulated data. The Figure 8 indicates that, there are still some considerable dependence between the subprocesses at difference scales

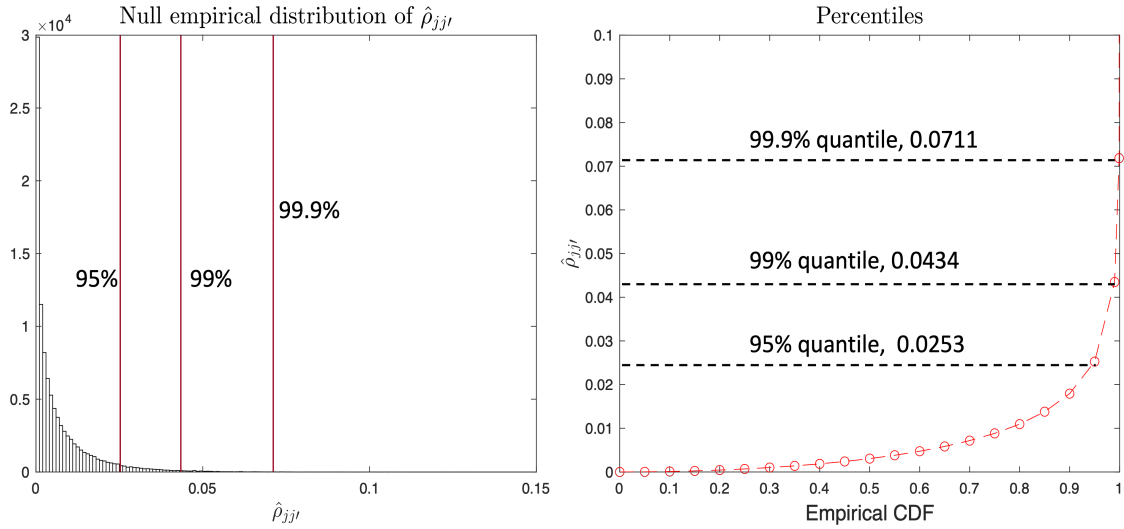


Figure 7: The left figure shows the null empirical distribution of $\hat{\rho}_{jj'}$ from 100,000 iterations with the simulation data; the right figure shows the percentiles of empirical cumulative distribution function (CDF) of $\hat{\rho}_{jj'}$ with the thresholds at 95%, 99% and 99.9% respectively.

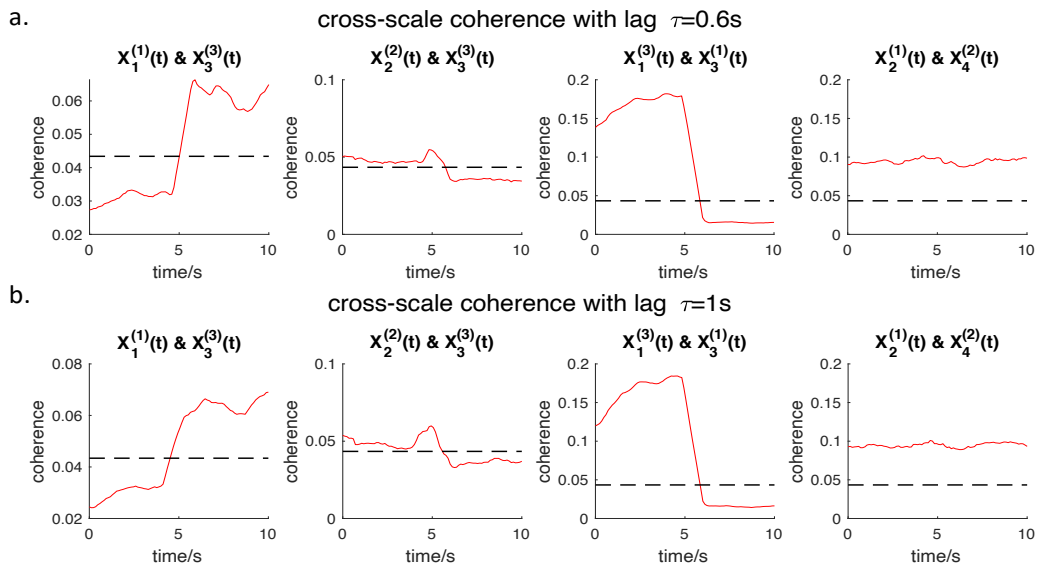


Figure 8: (a) shows mean of truth coherence (red solid) with a 0.6 second lag between some subprocesses at the different scales obtained from 100 simulations, and the dotted lines denote the threshold under 99% confidence level. (b) shows that with a 1 second lag.

with time lags, although some of them are weaker than that without lag, which means our framework can capture the short- and long-term dynamics relationship of the multivariate time series. For further determining the effect of the proposed model, the partial cross-scale coherence is calculated to check if there is direct dependence when the subprocesses have time lags. The Figure 9 shows that the partial dependence structure is similar to the regular cross-scale coherence. The results of simulation study can verify the framework holds in practice.

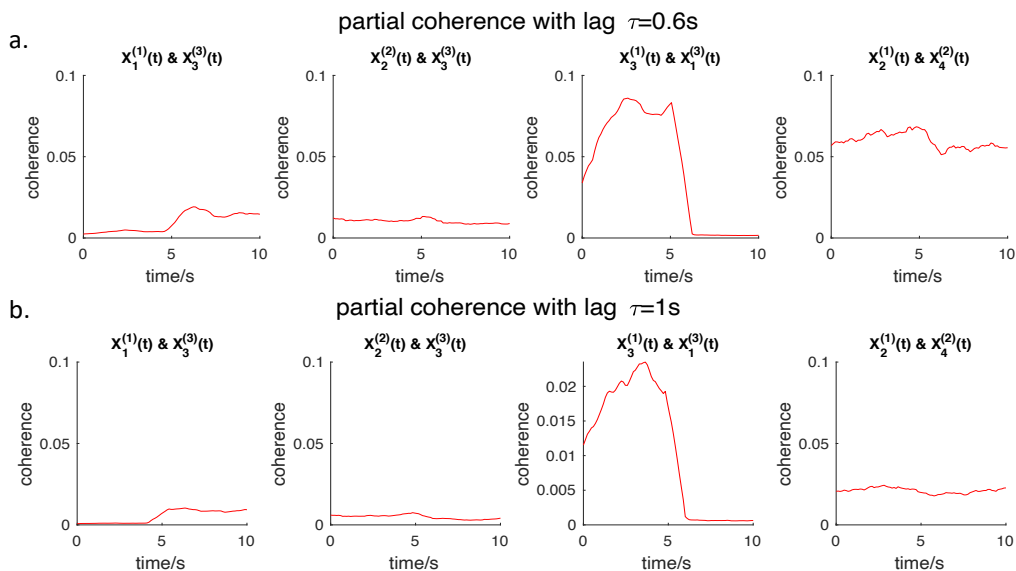


Figure 9: (a) shows mean of truth partial-coherence(red solid) with a 0.6 second lag between some subprocesses at the different scales obtained from 100 simulations. (b) shows that with a 1 second lag.

4 Data analysis

To further investigate the performance of the proposed measurement methodology, we now consider two examples. In Section 4.1 we perform the MvLSW process with cross-scale dependence on multivariate EEG data recorded from some ADHD and control subjects.

Section 4.2 presents an analysis of stock returns of some well-known companies.

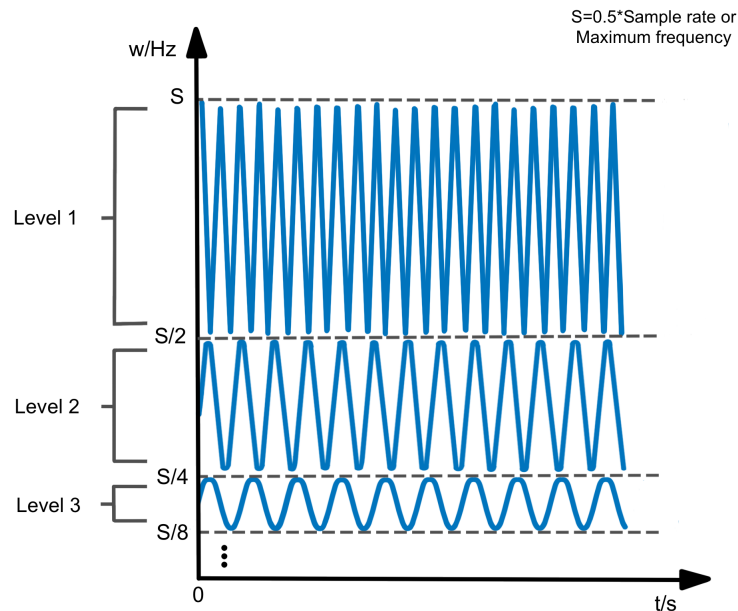


Figure 10: The corresponding relations between the scale and frequency band of components at every scale in terms of the sampling rate and maximum frequency of the original signal.

4.1 EEG data analysis

Our main goal is to study cross-channel dependence in a brain network. In particular, we would like to develop a method that can be used to study interactions between long-term dynamics in one channel and short-term dynamics in another. Here, the dataset is a 19-channel EEG recorded at a sample rate of 128 Hertz and then apply 5-th order Butterworth band-pass filters to segment the signal into the main “brain rhythms”, i.e, frequency components into the delta band $(0.5, 4.0)Hz$, theta band $(4.0, 8.0)Hz$, alpha band $(8.0, 12.0)Hz$, beta band $(12.0, 30.0)Hz$, and gamma band $(30.0, 50.0)Hz$. In this paper, we selected data for 23 subjects from ADHD group and 16 subjects from control

group, and used 4 channels namely Fp1 (fronto-central region), Fp2 (fronto-central region), O1 (occipital region) and O2 (also occipital region). Here we demonstrate the analysis of

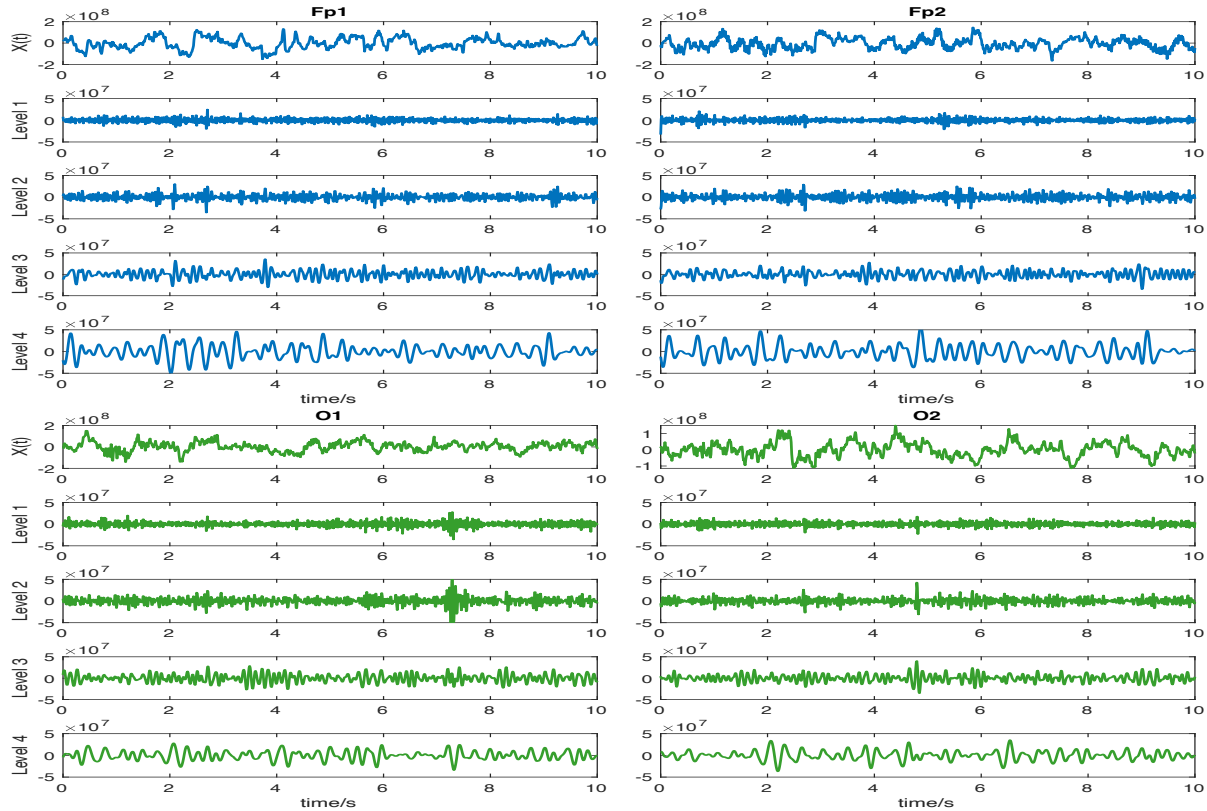


Figure 11: The realization of Fp1, Fp2, O1, O2 and their subprocesses at every scale.

cross-scale dependence of the signals from these channels under our proposed framework. Due to the low and high pass quadrature mirror filters that used in the decomposition and reconstruction of the Daubechies (1992). The wavelet spectral of the subprocess at every scale has particular corresponding relations with the frequency bands (see Figure 10).

Specifically, for this dataset and we use the decomposition level $J = 4$ and we have $j = 1(25 - 50Hz)$, $j = 2(12.5 - 25Hz)$, $j = 3(6.25 - 12.5Hz)$ and $j = 4(3.125 - 6.25Hz)$. The realizations of signals from Fp1, Fp2, O1, O2 and their subprocess at each scale are shown in Figure 11. Figure 12 shows the time-varying spectrum of these subprocesses, which indicates the components of signals from these channels at corresponding frequency

band can be captured by the scale-specific subprocesses.

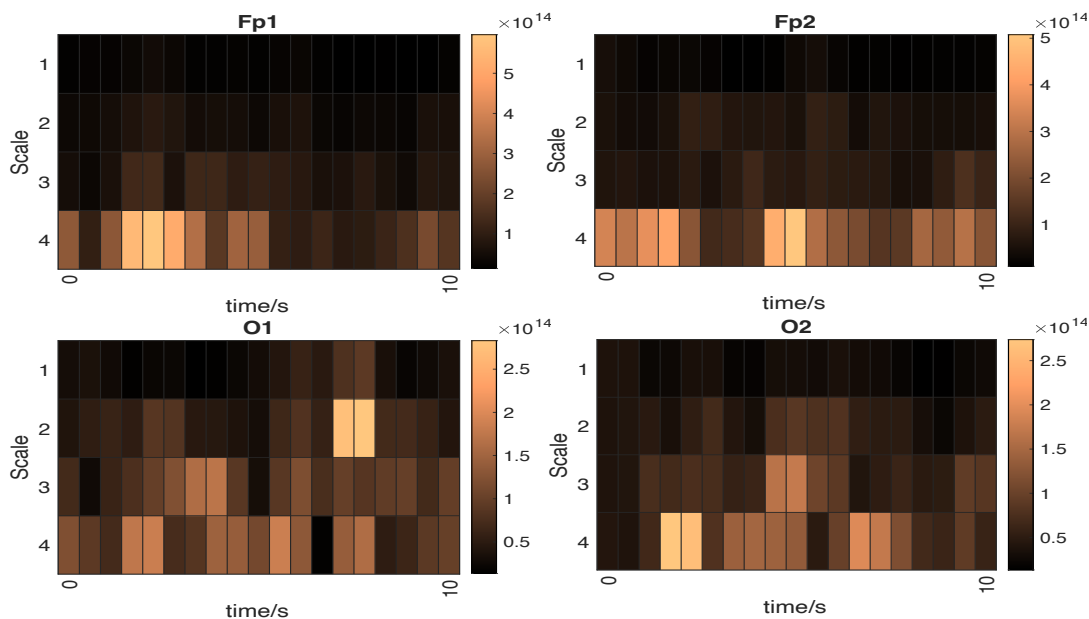


Figure 12: The time-varying spectrum of subprocesses of Fp1, Fp2, O1, O2 at scale 1, 2, 3 and 4, it shows distribution of power of the signal varying across time at different scales.

To study the dynamics within each brain region, we calculated the time-evolving single- and cross- scale dependence among these signals and the subprocesses, using a smoothing moving window. The Daubechies nonlinear-phase wavelet with 2 vanishing moments was used as the analyzing wavelet, which can capture the local and time-varying features of the signal. Figure 13(a) shows the sample mean of single-scale coherence results among 23 ADHD subjects and 16 control subjects, between four pairs of subprocess from the four channels. We use $X_j^{(p)}$ denotes the scale- j subprocess of signal from channel p . The results of coherence between $X_1^{(Fp1)}$ and $X_1^{(Fp2)}$ suggests that brain activity at the conventional gamma band captured by Fp1 exhibited linear dependence with Fp2. The interaction between these two channels much stronger at scale-3 (within in theta and alpha bands). The time-varying dependence structure was also found between the brain activity in occipital region O1, O2, the cross-scale dependence between the subprocess of O1, O2 at given pair

of scale evolves over time.

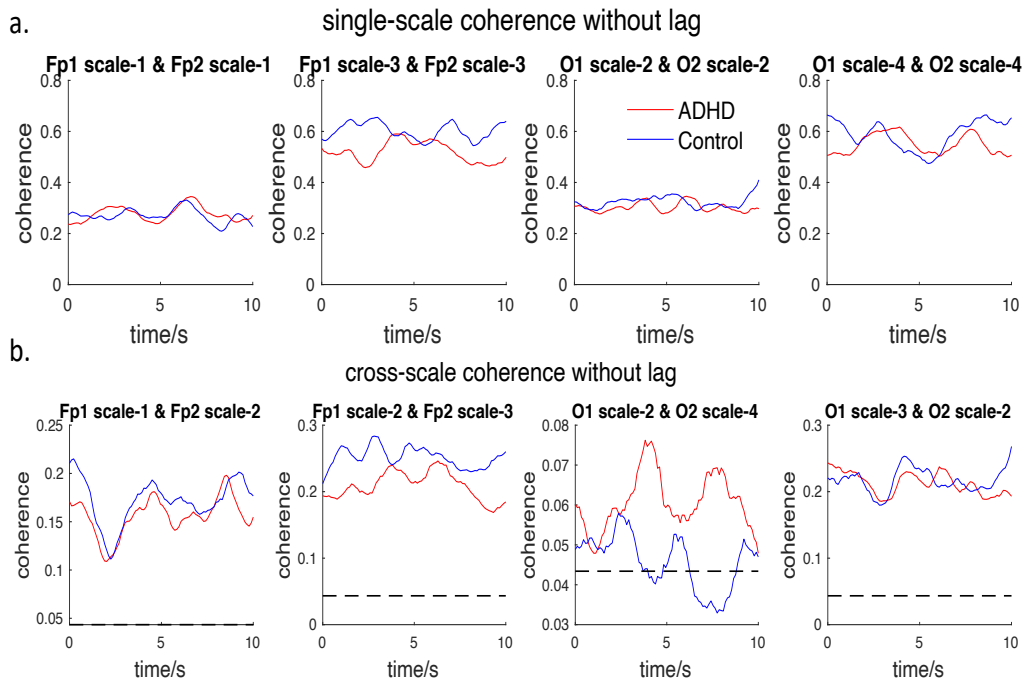


Figure 13: (a) shows the mean of truth coherence (red solid line for ADHD, blue solid line for control) between the subprocesses at same scales; (b) shows that of different scales and the dotted lines denote the threshold under 99% confidence level.

In contrast, the dynamics of cross-scale dependence with the brain network was measured by cross-scale wavelet coherence. The plots displaying confidence bands on the wavelet coherence (see Figure 13(b)) illustrate that, for most part, there is a cross-scale dependence between the signals from channel Fp1 and Fp2 captured by scale-2 component of Fp1, $X_2^{(Fp1)}$, and scale-3 component of Fp2, $X_3^{(Fp2)}$, which means that the brain activity at gamma band in Fp1 has dynamical impact on that at beta band in Fp2. The coherence in control group is higher than that in ADHD group at most of time. For the results of O1 and O2, brain activity capture by the scale-2 component of O1 channel, $X_2^{(O1)}$, exhibited no significant linear dependence with that of scale-4 component of O2 channel, $X_4^{(O2)}$. However, the cross-scale dependence between scale-3 component of O1, $X_3^{(O1)}$, and

scale-2 component of O2, $X_2^{(O2)}$, can be captured by the measurement, it indicates that there are significant interactions between components of O1 at the band of $6.25 - 12.5Hz$ and components of O2 at the band of $12.5 - 25Hz$. Similar to the simulation study, we

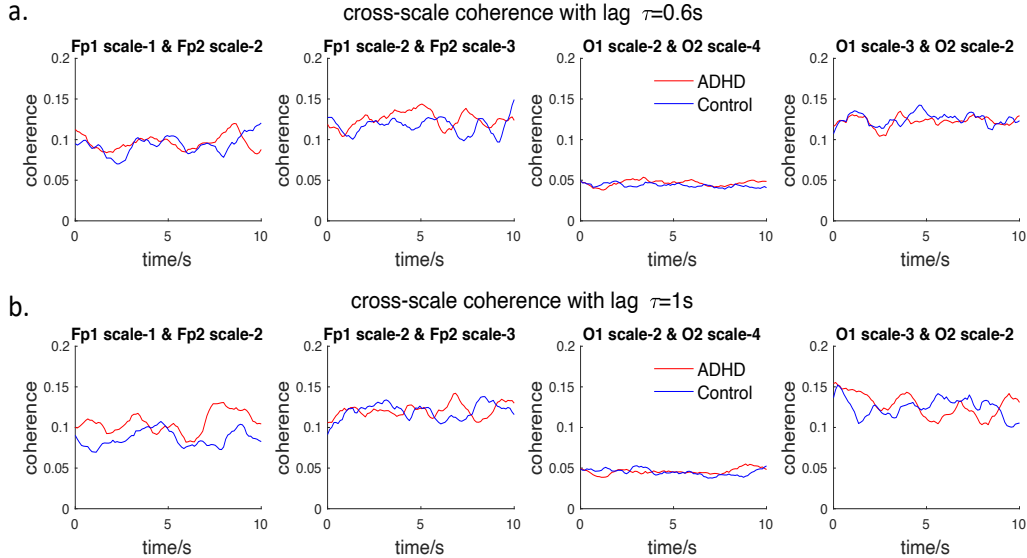


Figure 14: (a) shows the mean of cross-scale coherence with 0.6 second lag (red solid line for ADHD, blue solid line for control) between the subprocesses at given scales; (b) shows that with 1 second lag.

study the cross-scale dependence structure between the subprocesses with time lags (See Figure 14), and the results shows the dependence is still strong, it becomes much weaker in partial cross-scale coherence (Figure 15) when we controlled the time periods between the selected subprocess, but the dependence is still significant for some pair of subprocesses ($X_2^{(Fp1)}$ and $X_3^{(Fp2)}$).

The follow-up question is whether or not the cross-scale dependence between these scale-specific subprocesses can help us to identify some different cross-scale interactions between the ADHD and control group. We address this question by calculating the above four pairs of cross-scale coherence for all 23 ADHD subjects and 16 control subjects. We used

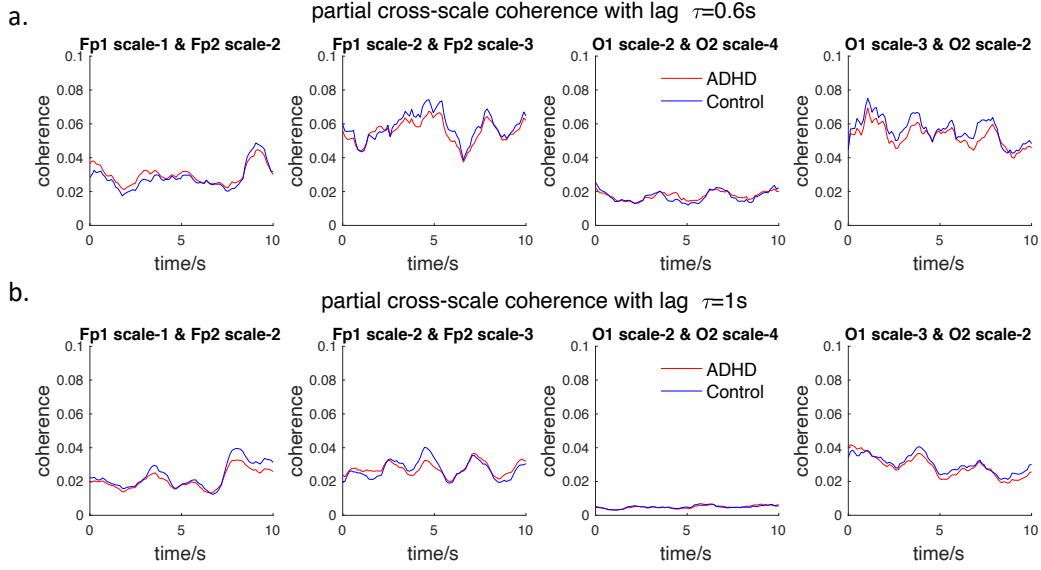


Figure 15: (a) shows the mean of partial cross-scale coherence with 0.6 second lag (red solid line for ADHD, blue solid line for control) between the subprocesses at given scales; (b) shows that with 1 second lag.

permutation test (random permutation 10,000 times), permutating the coherence between the given subprocesses for all of subjects in ADHD and healthy control group, based on the medians of cross-scale coherence from two groups, to determine if the coherence, $\rho_{jj'}$, of ADHD and control come from the same distribution. The statistics is $T = \sum_t (\hat{\rho}_{med}^{(1)}(t) - \hat{\rho}_{med}^{(2)}(t))^2$, where $\hat{\rho}_{med}^{(1)}$, $\hat{\rho}_{med}^{(2)}$ denotes the median coherence of ADHD and control respectively.

Figure 16 shows the histogram of permutation test statistics T of four pairs cross-scale coherence and the location of the observed statistics value T_{obs} , which suggests that the dependence between $X_2^{(Fp1)}(t)$ and $X_3^{(Fp2)}(t)$ in ADHD group has a significant difference (p -value < 0.05) with that in control group, illustrating that there is a functional connectivity alternation in children with ADHD between these two brain regions at corresponding working frequency bands ($6.25 - 12.5Hz$ and $12.5 - 25Hz$). The cross-scale dependence between $X_2^{(O1)}(t)$ ($12.5 - 25Hz$) and $X_4^{(O2)}(t)$ ($3.125 - 6.25Hz$). By calculating the cross-scale depen-

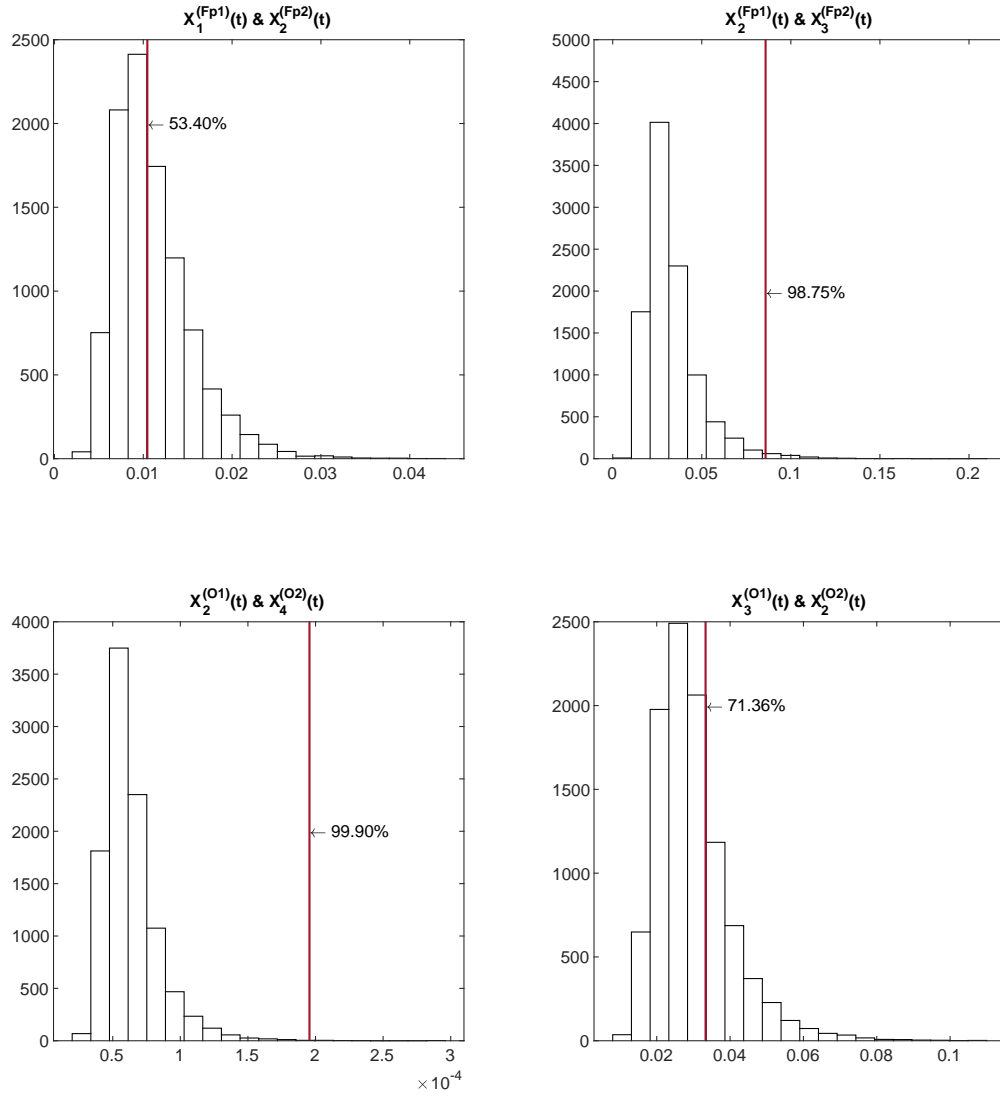


Figure 16: The histogram of T statistics from 10,000 times permutation test, the red line indicates the location of observed (truth) statistics value, and the quantiles of these observed statistics. For this figure, p -value = 0.466, 0.0125, 0.001 and 0.2864 respectively.

dence and comparing the results of ADHD and control with permutation test, we get the scale-specific brain dynamic patterns for selected six channels (see Figure 17) to illustrate the alterations in functional connectivity structure in children with ADHD. The results in

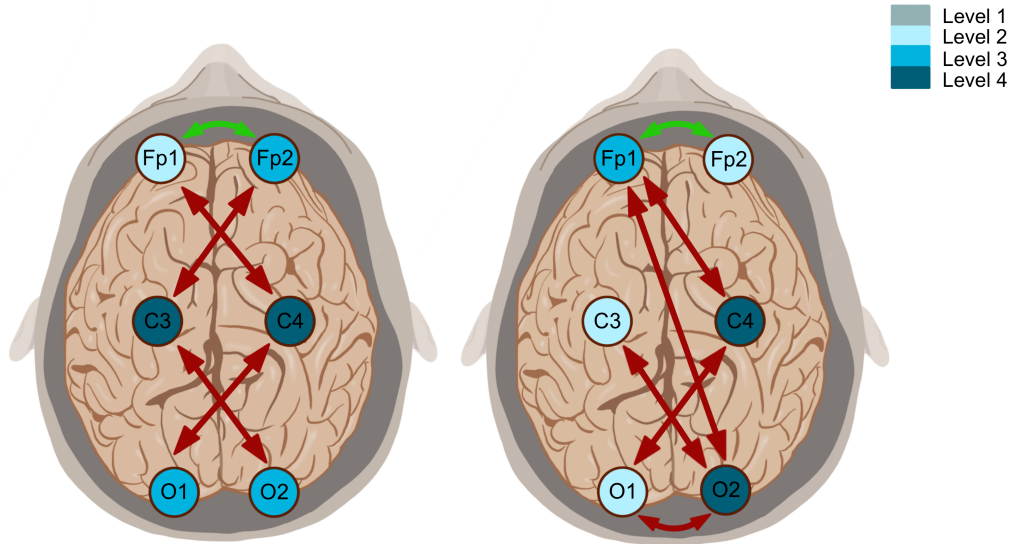


Figure 17: The red arrow denotes the cross-scale dependence between the channels in ADHD is stronger than that of control, the green arrow denotes the cross-scale dependence between the channels in ADHD is weaker than that of control.

Figure 17 indicate that functional connectivity in children with ADHD has many significant alterations comparing to control according to the permutation test. Within selected 6 channels, most of the connectivity between the scale-specific components in ADHD is much stronger than that in control. However, the connectivity between $X_2^{(Fp1)}$ and $X_3^{(Fp2)}$, $X_3^{(Fp1)}$ and $X_2^{(Fp2)}$ becomes weaker when children have ADHD, which means that the interactions between the activities from Fp1 and Fp2 in beta and alpha band are less than control.

4.2 Financial data analysis

To further investigate the effects of our framework and explore much more potential cross-scale dependence structure in actual non-stationary time series. We provide an additional example by using the model on the high frequency financial data. The dataset we analyze here is the daily stock prices of some large companies in the US from 2013 to 2017. Moreover, we choose four companies, with two of them from technology field (Apple and Microsoft), two of them from energy (ConocoPhillips and CMS Energy Corporation). We calculate the rate of return of these stocks with the close prices every day (see Figure 18). Specifically, we use the logarithmic return, R , with the form as,

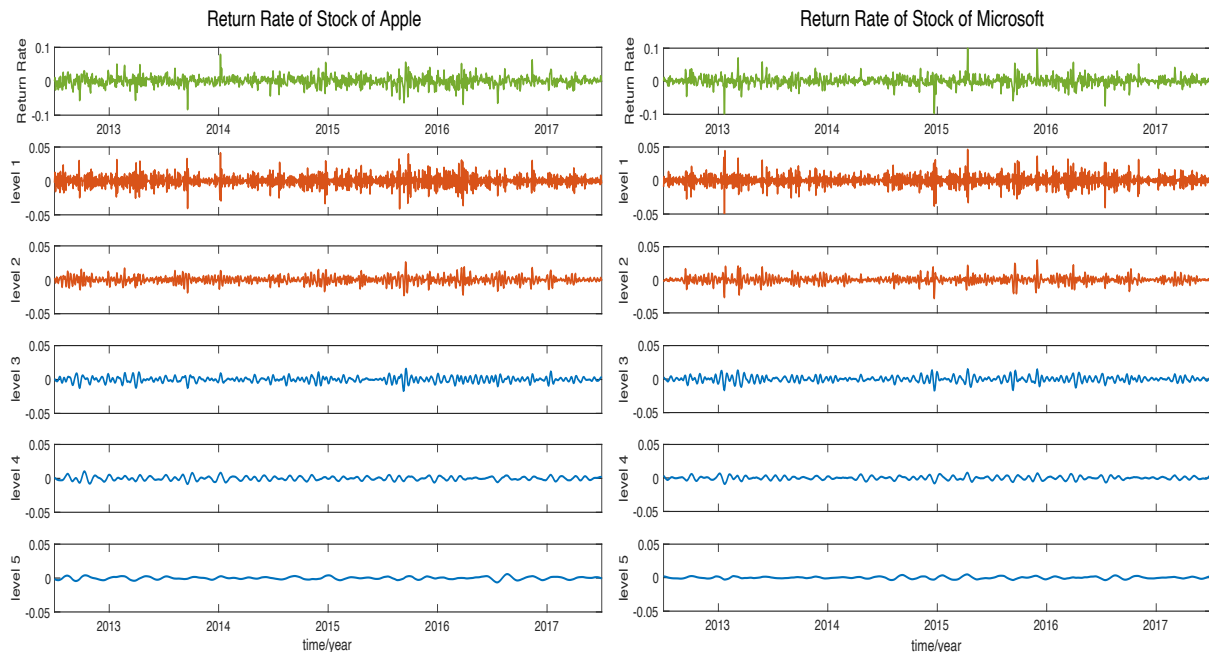


Figure 18: The return rate of the stock of Apple and Microsoft from 2013 to 2017.

$$R = \frac{\ln\left(\frac{V_f}{V_i}\right)}{n} \times 100\%$$

where V_i is the initial value of the investment, V_f is the final value and n is the number of time periods. The equivalent sampling rate in this data is around 365 because we have 365 time points per year. Hence, the subprocess at level 1 contains information in 1 cycle with 4 days to 1 cycle with 2 days, the subprocess at level 2 contains information in 1 cycle with 8 days to 1 cycle with 4 days, the subprocesses at other levels also follows the rule shown in Figure 10.

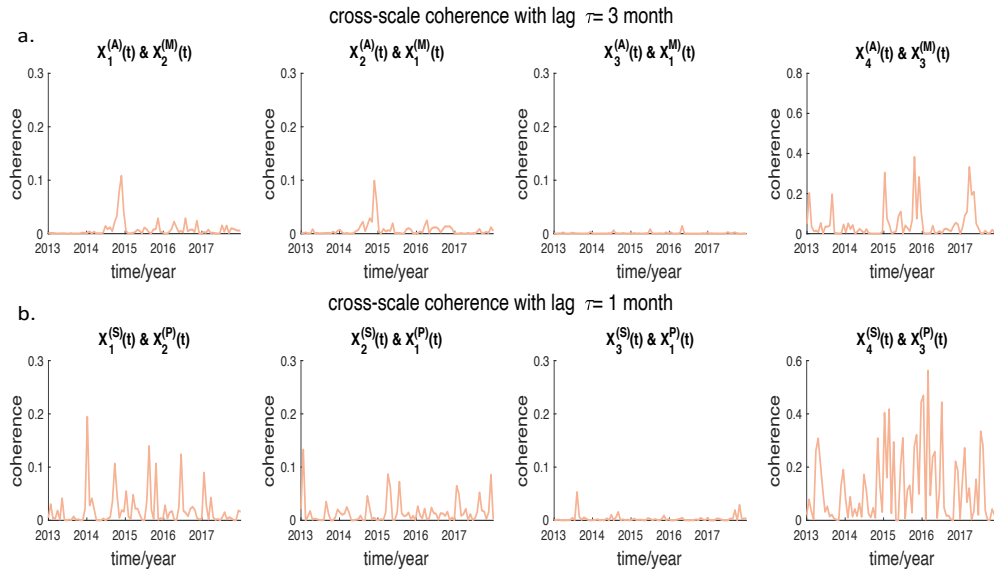


Figure 19: (a) The cross-scale coherence with 3 months lag between the return-rate of Apple ($X^{(A)}(t)$) and Microsoft ($X^{(M)}(t)$); The cross-scale coherence with 1 month lag between the return-rate of CMS Energy Corporation ($X^{(S)}(t)$) and ConocoPhillips ($X^{(P)}(t)$).

To study the how the return rate of one stock may have an long or short term impact on the return rate of another stock, we calculate the cross-scale coherence between the subprocesses of the selected companies. Figure 19(a) indicates that for most of time periods from 2013 to 2017, there is weak cross-scale dependence between $X_1^{(A)}$ and $X_2^{(M)}$, similar between $X_2^{(A)}$ and $X_1^{(M)}$. Hence, the return rate in a cycle within 4-8 days has weak impact on the return rate in a cycle within 2-4 days for the stocks of Apple and Microsoft for the

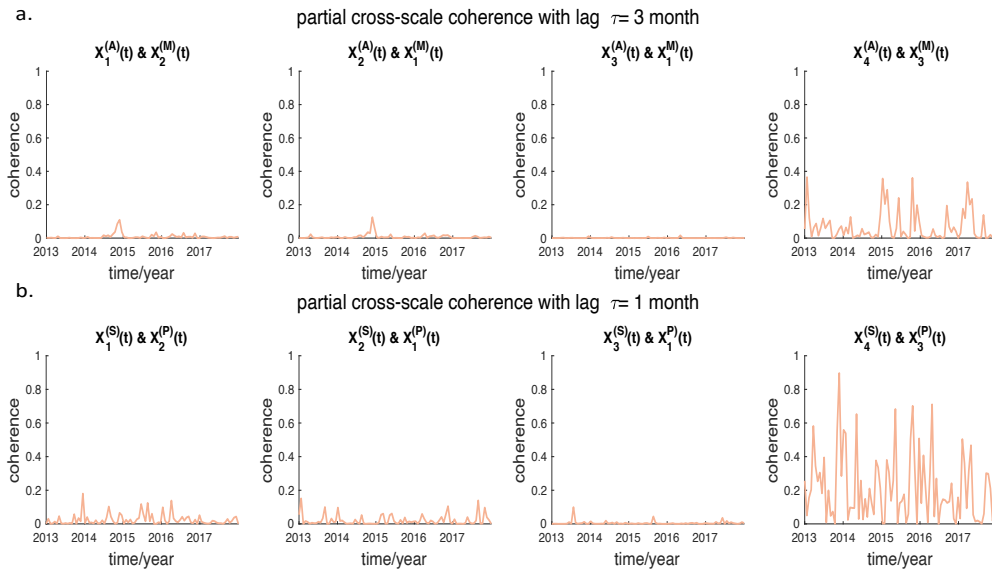


Figure 20: (a) The partial cross-scale coherence with 3 months lag between the return-rate of Apple ($X^{(A)}(t)$) and Microsoft ($X^{(M)}(t)$); (b) The partial cross-scale coherence with 1 month lag between the return-rate of CMS Energy Corporation ($X^{(S)}(t)$) and ConocoPhillips ($X^{(P)}(t)$).

future 3 months. In almost all of the time from 2013 to 2017, the cross-scale coherence between $X_3^{(A)}$ and $X_1^{(M)}$ is approximating to 0, which means that the return rate of Apple's stock in a cycle within around one week to half a month has no linear impact on the weekly return rate of Microsoft's stock. However, cross-scale coherence between $X_4^{(A)}$ and $X_3^{(M)}$ is much stronger in many time periods within the five years, the results indicate that the monthly return rate of the stock of Apple has strong influence on weekly to half-monthly return rate of the stock of Microsoft. The similar dynamical relationship between the return rate of CMS Energy Corporation and ConocoPhillips appears in Figure 19(b). The above results show that the return rate of the stocks from different sectors not only has daily impact on each other, it may exhibit stronger dependence over the longer time periods. The Figure 20 shows that it is difficult to predict the future (more than 1 month) return directly with the proposed framework, which is one of the drawbacks.

5 Conclusion

In this paper, we developed a rigorous multi-resolution analysis-based wavelets modeling framework, which can capture time-evolutionary cross-scale dependence between components of multivariate time series. This contribution is significant because it can be used by neuroscientists to investigate associations between long-term dynamics in one channel and short-term dynamics in another. Another contribution in this paper is a formal definition of this cross-scale dependence and the associated theory with the estimation procedure. The particular construction is we concentrate on the dependence structure of the subprocesses at different scales. The results in EEG analysis shows that there are many time-evolving cross-scale dependence between the channels in brain activity. The performing of the estimation theory on EEG ADHD data validates the effects of our proposed estimator. Using

the proposed cross-scale wavelet coherence analysis, our method produced novel and interesting results when we compared the brain networks of healthy control children and that of the ADHD population. In particular, our method showed that the connectivity between many of given pair of channels and scales in children with ADHD is much stronger than that of control, and the connectivity in fronto-central region at beta and alpha bands is weaker in children with ADHD. These results are interesting and could lead to new investigations in the field of ADHD and other neurological diseases. Our cross-scale coherence method has potential impact beyond brain networks. We also applied this to financial data to examine how short-term dynamics (hourly) can have an impact on longer-term dynamics (daily, weekly, monthly). The findings are intriguing in a sense that the change in one stock on a given day might have weeks or months of effects on another stock. The application of the framework to the financial data demonstrates the generalization ability of the model and shows that the cross-scale dependence structure could be ubiquitous in natural data.

References

- Basu, S., S. Das, G. Michailidis, and A. Purnanandam (2019). A system-wide approach to measure connectivity in the financial sector. *Social Science Research Network*.
- Brassarote, G., E. Souza, and J. Monico (2018). Non-decimated wavelet transform for a shift-invariant analysis. *Trends in Computational and Applied Mathematics* 19(1), 93.
- Dahlhaus, R. (1997). Fitting time series models to nonstationary processes. *The Annals of Statistics* 25(1), 1–37.
- Daubechies, I. (1992). *Ten lectures on wavelets*. SIAM.
- Embleton, J., M. Knight, and H. Ombao (2022). Multiscale spectral modelling for non-stationary time series within an ordered multiple-trial experiment. *Annals of Applied Statistics* 16(4), 2774–2803.
- Fiecas, M. and H. Ombao (2016). Modeling the evolution of dynamic brain processes during an associative learning experiment. *Journal of the American Statistical Association* 111(516), 1440–1453.
- Isserlis, L. (1918). On a formula for the product-moment coefficient of any order of a normal frequency distribution in any number of variables. *Biometrika* 12(1/2), 134–139.
- Koopmans, L. (1964). On the multivariate analysis of weakly stationary stochastic processes. *The Annals of Mathematical Statistics* 35(4), 1765–1780.
- Motie Nasrabadi, A., A. Allahverdy, M. Samavati, and M. R. Mohammadi (2020). Eeg data for adhd / control children.

Nason, G., R. Sachs, and G. Kroisandt (2000). Wavelet processes and adaptive estimation of the evolutionary wavelet spectrum. *Journal of the Royal Statistical Society: Series B (Statistical Methodology)* 62(2), 271–292.

Ombao, H., R. Sachs, and W. Guo (2005). Slex analysis of multivariate nonstationary time series. *Journal of the American Statistical Association* 100(470), 519–531.

Park, T., I. Eckley, and H. Ombao (2014). Estimating time-evolving partial coherence between signals via multivariate locally stationary wavelet processes. *IEEE Transactions on Signal Processing* 62, 5240–5250.

Priestley, M. B. (1981). *Spectral analysis and time series / M.B. Priestley*. Academic Press London ; New York.

Sanderson, J., P. Fryzlewicz, and M. W. Jones (2010). Estimating linear dependence between nonstationary time series using the locally stationary wavelet model. *Biometrika* 97(2), 435–446.

A

PROOF OF PROPOSITION 1:

Recalling the representation of a scale- j component of the P -variate locally stationary wavelet process in (4) yields

$$\begin{aligned}
\text{cov}(X_{j,[uT]}^{(p)}, X_{j,[uT]+\tau}^{(q)}) &= E \left[X_{j,[uT]}^{(p)} X_{j,[uT]+\tau}^{(q)} \right] \\
&= E \left[\sum_k \mathbf{V}_j^{(p)}(k/T) \psi_{j,k}([uT]) \mathbf{z}_{j,k} \times \left(\sum_{k'} \mathbf{V}_j^{(q)}(k'/T) \psi_{j,k'}([uT] + \tau) \mathbf{z}_{j,k'} \right) \right] \\
&= \sum_k \sum_{k'} \mathbf{V}_j^{(p)}(k/T) \psi_{j,k}([uT]) E[\mathbf{z}_{j,k} \mathbf{z}_{j,k'}'] \psi_{j,k'}([uT] + \tau) \mathbf{V}_j^{(q)}(k'/T),
\end{aligned}$$

where $\mathbf{V}_j^{(p)}(u)$ is the p th row of the $\mathbf{V}_j(u)$ transfer matrix of $\{X_{t:T}\}$.

Recalling the assumptions about the random vectors, $E[\mathbf{z}_{j,k}\mathbf{z}'_{j,k'}] = \text{cov}(\mathbf{z}_{j,k}, \mathbf{z}_{j,k'}) = \boldsymbol{\rho}_{j,j;k}\delta_{k,k'}$, where $\boldsymbol{\rho}_{j,j;k} = \mathbf{I}$, which is a identity matrix if and only if $k = k'$, $\delta_{k,k'} = 1$ and using the definition of the LWS matrix, $S_j^{(p,q)}(u) = \mathbf{V}_j^p(u)\mathbf{V}_j^{\prime q}(u)$, letting $m = k - [uT]$ we obtain

$$\text{cov}(X_{j,[uT]}^{(p)}, X_{j,[uT]+\tau}^{(q)}) = \sum_m S_j^{(p,q)}\left(\frac{[uT] + m}{T}\right) \psi_{j,m}(0)\psi_{j,m}(\tau)$$

Analogous to the method proposed by Koopmans (1964), using the Lipschitz continuous property of $V_j^{(p,q)}(u)$ and therefore of $S_j^{(p,q)}(u)$, we consider the difference between this covariance and the function $c_j^{(p,q)}(u, \tau)$,

$$\begin{aligned} & \left| \text{cov}(X_{j,[uT]}^{(p)}, X_{j,[uT]+\tau}^{(q)}) - c_j^{(p,q)}(u, \tau) \right| \\ &= \left| \sum_m S_j^{(p,q)}\left(\frac{[uT] + m}{T}\right) \psi_{j,m}(0)\psi_{j,m}(\tau) - c_j^{(p,q)}(u, \tau) \right| \\ &\leq T^{-1} \sum_m |m|L_j|\psi_{j,m}(0)\psi_{j,m}(\tau)| = \mathcal{O}(T^{-1}). \end{aligned}$$

Similarly,

$$\begin{aligned} \text{cov}(X_{j,[uT]}^{(p)}, X_{j',[uT]+\tau}^{(q)}) &= E \left[X_{j,[uT]}^{(p)} X_{j',[uT]+\tau}^{\prime(q)} \right] \\ &= E \left[\sum_k \mathbf{V}_j^{(p)}(k/T) \psi_{j,k}([uT]) \mathbf{z}_{j,k} \times \left(\sum_{k'} \mathbf{V}_{j'}^{(q)}(k'/T) \psi_{j',k'}([uT] + \tau) \mathbf{z}_{j',k'} \right)' \right] \\ &= \sum_k \sum_{k'} \mathbf{V}_j^{(p)}(k/T) \psi_{j,k}([uT]) E[\mathbf{z}_{j,k} \mathbf{z}'_{j',k'}] \psi_{j',k'}([uT] + \tau) \mathbf{V}_{j'}^{\prime(q)}(k'/T), \end{aligned}$$

where $E[\mathbf{z}_{j,k}\mathbf{z}'_{j',k'}] = \text{cov}(\mathbf{z}_{j,k}, \mathbf{z}_{j',k'}) = \boldsymbol{\rho}_{j,j';k}\delta_{k,k'}$, and if and only if $k = k'$, $\delta_{k,k'} = 1$. From the definition of the cross-scale LWS matrix, $S_{jj'}^{(p,q)}(u) = \mathbf{V}_j^{(p)}(u)\boldsymbol{\rho}_{jj'}^{(p,q)}(u)\mathbf{V}_{j'}^{\prime(q)}(u)$, suppose that $m = k - uT$, then

$$\text{cov}(X_{j,[uT]}^{(p)}, X_{j',[uT]+\tau}^{(q)}) = \sum_m S_{jj'}^{(p,q)}\left(\frac{[uT] + m}{T}\right) \psi_{j,m}(0)\psi_{j',m}(\tau)$$

Using the assumption of Lipschitz continuity of $V_j^{(p,q)}(u)$ and therefore of $S_{jj'}^{(p,q)}(u)$, we consider the difference between this covariance and the function $c_{jj'}^{(p,q)}(u, \tau)$,

$$\begin{aligned} & \left| \text{cov}(X_{j,[uT]}^{(p)}, X_{j',[uT]+\tau}^{(q)}) - c_{jj'}^{(p,q)}(u, \tau) \right| \\ &= \left| \sum_m S_{jj'}^{(p,q)} \left(\frac{[uT] + m}{T} \right) \psi_{j,m}(0) \psi_{j',m}(\tau) - c_{jj'}^{(p,q)}(u, \tau) \right| \\ &\leq T^{-1} \sum_m |m| L_j |\psi_{j,m}(0) \psi_{j',m}(\tau)| = \mathcal{O}(T^{-1}). \end{aligned}$$

PROOF OF PROPOSITION 2:

Recall that $\mathbf{d}_{j,k}^{(p)} = \sum_t \mathbf{X}_{t;T}^{(p)} \psi_{j,k}(t)$ where $\mathbf{X}_{t;T}^{(p)} = \sum_l \sum_m \mathbf{V}_l^{(p)}(m/T) \psi_{l,m} \mathbf{z}_{l,m}$, and similarly for the q th channel. Thus

$$\begin{aligned} E[I_{jj',kk'}^{(p,q)}] &= E \left[\left\{ \sum_t X_{t;T}^{(p)} \psi_{j,k}(t) \right\} \left\{ \sum_{t'} X_{t';T}^{(q)} \psi_{j',k'}(t') \right\} \right] \\ &= \sum_l \sum_{l'} \sum_m \mathbf{V}_l^{(p)}(m/T) \rho_{ll'}(m/T) \mathbf{V}_{l'}^{(q)}(m/T) \\ &\quad \times \left\{ \sum_t \psi_{l,m}(t) \psi_{j,k}(t) \sum_{t'} \psi_{l',m}(t') \psi_{j',k'}(t') \right\} \end{aligned} \quad (17)$$

Letting $m = n + k$ and substituting it into (A.1), we have

$$E[I_{jj',kk'}^{(p,q)}] = \sum_l \sum_{l'} \sum_n \left\{ S_{ll'}^{(p,q)} \left(\frac{n+k}{T} \right) \right\} \left\{ \sum_t \psi_{l,n+k-t} \psi_{j,k-t} \sum_{t'} \psi_{l',n+k-t'} \psi_{j',k'-t'} \right\}$$

Since $S_{jj'}^{(p,q)}(z)$ is Lipschitz continuous with finite Lipschitz constant $L_{jj'}^{(p,q)}$, for some fixed

n , $\left| S_{jj'}^{(p,q)}((n+k)/T) - S_{jj'}^{(p,q)}(k/T) \right| \leq |n| L_{jj'}^{(p,q)} / T$ and we obtain

$$E[I_{jj',kk'}^{(p,q)}] = \sum_l \sum_{l'} S_{ll'}^{(p,q)}(k/T) \sum_n \left\{ \sum_t \psi_{l,n+k-t} \psi_{j,k-t} \right\} \times \left\{ \sum_{t'} \psi_{l',n+k-t'} \psi_{j',k'-t'} \right\} + \mathcal{O}(T^{-1}).$$

From the definition of the cross-scale autocorrelation wavelets we find that,

$$\begin{aligned}
E[I_{jj',kk'}^{(p,q)}] &= \sum_l \sum_{l'} S_{l'}^{(p,q)}(k/T) \sum_n \Psi_{lj}(n) \Psi_{l'j'}(n+k-k') + \mathcal{O}(T^{-1}) \\
&= \sum_l \sum_{l'} A_{l';jj'}^{k-k'} S_{l'}^{(p,q)}(k/T) + \mathcal{O}(T^{-1}).
\end{aligned} \tag{18}$$

For the variance, we start by considering $E \left[(I_{jj',kk'}^{(p,q)})^2 \right] = E \left[(d_{j,k}^{(p)})^2 (d_{j',k'}^{(q)})^2 \right]$.

$$\begin{aligned}
E \left[(I_{jj',kk'}^{(p,q)})^2 \right] &= \left(\sum_l \sum_m V_l^{(p)}(m/T) \sum_t \psi_{l,m}(t) \psi_{j,k}(t) \right. \\
&\quad \times \left. \sum_{l'} \sum_{m'} V_{l'}^{(q)}(m'/T) \sum_{t'} \psi_{l',m'}(t') \psi_{j',k'}(t') \right)^2 \\
&\quad \times E [z_{l_1,m_1} z_{l_2,m_2} z_{l_3,m_3} z_{l_4,m_4}].
\end{aligned}$$

Using the result derived by Isserlis (1918) the above formation can be re-written to the sum of three different terms as $E \left[(I_{jj',kk'}^{(p,q)})^2 \right] = I_1 + I_2 + I_3$, where,

$$I_1 = \prod_{i=1}^4 \sum_{l_i, m_i} V_{l_i}^{p_i}(m_i/T) \psi_{l_i, m_i}(t_i) \psi_{j,k}(t_1) \psi_{j',k'}(t_2) \psi_{j,k}(t_3) \psi_{j',k'}(t_4) E [z_{l_1, m_1} z_{l_2, m_2}] E [z_{l_3, m_3} z_{l_4, m_4}].$$

Since $E [z_{l_1, m_1} z_{l_2, m_2}] = \delta_{m_1 m_2} \rho_{l_1 l_2}$, then,

$$\begin{aligned}
I_1 &= \sum_{l_1, l_2} \sum_{m_1} V_{l_1}^{(p)}(m_1/T) \rho_{l_1 l_2} V_{l_2}^{(p)}(m_1/T) \times \sum_{t_2=0}^{T-1} \psi_{l_1, m_1}(t_1) \psi_{j,k}(t_1) \\
&\quad \sum_{t_2=0}^{T-1} \psi_{l_2, m_1}(t_2) \psi_{j,k}(t_2) \sum_{l_3, l_4} \sum_{m_3} V_{l_3}^{(q)}(m_3/T) \rho_{l_3 l_4} V_{l_4}^{(q)}(m_3/T) \\
&\quad \sum_{t_3=0}^{T-1} \psi_{l_3, m_3}(t_3) \psi_{j,k}(t_3) \sum_{t_4=0}^{T-1} \psi_{l_4, m_3}(t_4) \psi_{j',k'}(t_4) \\
&= E \left[I_{jj',kk'}^{(p,p)} \right] E \left[I_{jj',kk'}^{(q,q)} \right].
\end{aligned}$$

Similarly for I_2 we get that $I_2 = E \left[I_{jj',kk'}^{(p,q)} \right]^2$ and $I_3 = E \left[I_{jj',kk'}^{(p,q)} \right]^2$. Thus,

$$E \left[\left(I_{jj',kk'}^{(p,q)} \right)^2 \right] = E \left[I_{jj',kk'}^{(p,p)} \right] E \left[I_{jj',kk'}^{(q,q)} \right] + 2E \left[I_{jj',kk'}^{(p,q)} \right]^2,$$

and

$$\begin{aligned} \text{var}(I_{jj',kk'}^{(p,q)}) &= \left(\sum_l \sum_{l'} A_{ll';jj'}^{k-k'} S_{ll'}^{(p,p)}(k/T) + \mathcal{O}(T^{-1}) \right) \\ &\quad \times \left(\sum_l \sum_{l'} A_{ll';jj'}^{k-k'} S_{ll'}^{(q,q)}(k/T) + \mathcal{O}(T^{-1}) \right) \\ &\quad + \left(\sum_l \sum_{l'} A_{ll';jj'}^{k-k'} S_{ll'}^{(p,q)}(k/T) + \mathcal{O}(T^{-1}) \right)^2. \end{aligned}$$

Nason et al. (2000) proved that $\sum_\tau |\Psi_j(\tau)| = \mathcal{O}(2^j)$, and Park et al. (2014) showed that $A_{jl} = \sum_\tau \Psi_j(\tau) \Psi_l(\tau) \leq (\sum_\tau |\Psi_j(\tau)|)^2 = \mathcal{O}(2^j)$, hence $A_{jj';ll'} = \sum_\tau \Psi_{jj'}(\tau) \Psi_{ll'}(\tau) \leq (\sum_\tau |\Psi_j(\tau)|)^2 = \mathcal{O}(2^j)$. Thus, it is easily to verify that,

$$\begin{aligned} \text{var}(I_{jj',kk';T}^{(p,q)}) &= \sum_l \sum_{l'} A_{ll';jj'}^{k-k'} S_{ll'}^{(p,p)}(k/T) \sum_l \sum_{l'} A_{ll';jj'}^{k-k'} S_{ll'}^{(q,q)}(k/T) \\ &\quad + \sum_l \sum_{l'} A_{ll';jj'}^{k-k'} S_{ll'}^{(p,q)}(k/T) + \mathcal{O}(2^{2j}/T). \end{aligned} \quad (19)$$

PROOF OF PROPOSITION 3:

Recall that the formation of the smoothed periodogram is, $\tilde{I}_{jj',kk'} = \frac{1}{2M+1} \sum_{m=-M}^M \mathbf{I}_{jj',(k+m)(k'+m)}$.

Expectation:

$$E \left[\tilde{I}_{jj',kk'}^{(p,q)} \right] = \frac{1}{2M+1} \sum_{m=-M}^M \left[I_{jj',(k+m)(k'+m)}^{(p,q)} \right]$$

where $2M+1$ is the length of the rectangular smoothing window. The expected value of this estimator can be derived to,

$$E \left[\tilde{I}_{jj',kk'}^{(p,q)} \right] = \frac{1}{2M+1} \sum_{m=-M}^M \sum_l \sum_{l'} \left\{ A_{ll';jj'}^{k-k'} S_{ll'}^{(p,q)} \left(\frac{k+m}{T} \right) + \mathcal{O}(T^{-1}) \right\}.$$

By the assumption of Lipschitz continuity for the spectral components which follows,

$$E \left[\tilde{I}_{jj',kk'}^{(p,q)} \right] = \sum_l \sum_{l'} A_{ll';jj'}^{k-k'} S_{ll'}^{(p,q)} \left(\frac{k}{T} \right) + \mathcal{O}(MT^{-1}).$$

As $T \rightarrow \infty, M \rightarrow \infty$ but $M/T \rightarrow 0$, the smoothed raw periodogram is asymptotically biased, which can be corrected to an asymptotically unbiased estimate by using the inverse inner product matrix, A^{-1} .

Variance: We begin by considering $E\left[(\tilde{I}_{jj',kk'}^{(p,q)})^2\right]$.

$$E\left[(\tilde{I}_{jj',kk'}^{(p,q)})^2\right] = \frac{1}{(2M+1)^2} \sum_{m=-M}^M \sum_{m'=-M}^M E\left[I_{jj',(k+m)(k'+m)}^{(p,q)} I_{jj',(k+m')(k'+m')}^{(p,q)}\right],$$

by substituting $\tau = m' - m$. Using arguments similar to those introduced in the proof of the Expectation, it follows that:

$$\begin{aligned} & \frac{1}{(2M+1)^2} \sum_{m=-M}^M \sum_{m'=-M}^M E\left[I_{jj',(k+m)(k'+m)}^{(p,q)} I_{jj',(k+m')(k'+m')}^{(p,q)}\right] \\ &= \frac{1}{(2M+1)^2} \sum_{m,\tau} E\left[d_{j,k+m}^{(p)} d_{j',k'+m}^{(q)} d_{j,k+m+\tau}^{(p)} d_{j',k'+m+\tau}^{(q)}\right] \end{aligned}$$

By the theorem in Isserlis (1918), the Variance of the smoothed periodogram can be shown that,

$$\begin{aligned} \text{var}\left(\tilde{I}_{jj',kk'}^{(p,q)}\right) &= \frac{1}{(2M+1)^2} \left\{ \sum_{m,\tau} E\left[d_{j,k+m}^{(p)} d_{j',k'+m}^{(q)}\right] \times E\left[d_{j',k'+m}^{(q)} d_{j,k+m+\tau}^{(p)}\right] \right. \\ &\quad \left. + \sum_{m,\tau} E\left[d_{j,k+m}^{(p)} d_{j',k'+m+\tau}^{(q)}\right] \times E\left[d_{j',k'+m}^{(q)} d_{j,k+m+\tau}^{(p)}\right] \right\}, \\ &= \frac{1}{(2M+1)^2} \sum_{m=-M}^M \left\{ \sum_{\tau} \sum_{l=1}^J S_l^{(p,p)}(k/T) A_{l,j}^{\tau} \times \sum_{l'=1}^J S_{l'}^{(q,q)}(k'/T) A_{l',j'}^{\tau} \right. \\ &\quad \left. + \sum_{\tau} \left(\sum_{l=1}^J \sum_{l'=1}^J S_{ll'}^{(p,q)}(k/T) A_{ll',jj'}^{k-k'} \right)^2 \right. \\ &\quad \left. + \sum_{\tau} (|\tau|+1) \mathcal{O}(T^{-1}) + \sum_{\tau} (|\tau|+1)^2 \mathcal{O}(T^{-2}) \right\} \end{aligned}$$

where $A_{l,j}^{\tau} = \sum_t \Psi_{l,j}(t) \Psi_{l,j}(t + \tau)$. $A_{l,j}^{\tau}$ is a inner product matrix with a given lag τ .

Examining the term,

$$\begin{aligned}
& \sum_{\tau} \sum_{l=1}^J S_l^{(p,p)}(k/T) A_{l,j}^{\tau} \sum_{l'=1}^J S_{l'}^{(q,q)}(k'/T) A_{l',j'}^{\tau} \\
& \leq \left(\sum_{\tau} \left| \sum_{l=1}^J S_l^{(p,p)}(k/T) A_{l,j}^{\tau} \right| \right) \left(\sum_{\tau} \left| \sum_{l'=1}^J S_{l'}^{(q,q)}(k'/T) A_{l',j'}^{\tau} \right| \right) \\
& = \mathcal{O}(2^{2j}) + \mathcal{O}(2^{2j'}).
\end{aligned}$$

Similarly it can be proved that the second term is also equal to $\mathcal{O}(2^{2j}) + \mathcal{O}(2^{2j'})$. Thus,

$$\text{var} \left(\tilde{I}_{jj',kk'}^{(p,q)} \right) = \mathcal{O}(2^{2j}/M) + \mathcal{O}(2^{2j}/T) + \mathcal{O}(2^{2j'}/M) + \mathcal{O}(2^{2j'}/T) \quad (20)$$

Hence, the smoothed wavelet periodogram is asymptotically mean-squared consistent as

$$T \rightarrow \infty, M \rightarrow \infty, \frac{M}{T} \rightarrow \infty.$$